

## 2. EXPLANATORY NOTES<sup>1</sup>

Shipboard Scientific Party<sup>2</sup>

### INTRODUCTION

The “Explanatory Notes” chapter is designed to document the primary procedures and methods employed by the scientists in the various shipboard laboratories in order to understand the basis for our preliminary interpretations of the cores and logging data. This information concerns only shipboard methods the results of which are presented in the site report from the Leg 203 *Initial Reports* volume. Methods for shore-based analysis of Leg 203 samples and data will be described in the individual scientific contributions to be published in scientific journals and the *Scientific Results* volume.

### Shipboard Scientific Procedures

#### Numbering of Sites, Holes, Cores, and Samples

Drilling sites are numbered consecutively, beginning with the first site drilled by the *Glomar Challenger* in 1968. At a site, multiple holes can be drilled by removing the drill pipe from the seafloor, moving the ship a short distance, and then drilling a new hole. For all Ocean Drilling Program (ODP) drill sites, a letter suffix distinguishes each hole drilled at the same site. The first hole drilled is assigned the site number modified by the suffix “A,” the second hole takes the site number and suffix “B,” and so forth.

The cored interval is measured in meters below seafloor (mbsf). The depth below seafloor is determined by subtracting the water depth estimated from the initial drill pipe measurement, which gives the length of pipe from the rig floor to the seafloor (measured in meters below rig floor) from the total drill pipe measurement. Each cored interval is generally 9.5–9.6 m long, which is the length of a core barrel. Coring inter-

<sup>1</sup>Examples of how to reference the whole or part of this volume.

<sup>2</sup>Shipboard Scientific Party addresses.

vals may be shorter and may not necessarily be adjacent if separated by drilled intervals.

A recovered core is divided into 1.5-m sections that are numbered serially from the top. When full recovery is obtained, the sections are numbered from one to seven, with the last section possibly being shorter than 1.5 m (Fig. F1). Occasionally, an unusually long core may require more than seven sections. When less than full recovery is obtained, there will be as many sections as needed to accommodate the length of the core recovered. By convention, material recovered from the core catcher (CC) of a sedimentary core is placed in a separate section during the core description, labeled CC, and placed below the last section recovered in the liner. The CC is placed at the top of the cored interval in cases where material is recovered only in the CC.

When the recovered core is shorter than the cored interval, the top of the core is equated with the top of the cored interval, by convention, in order to achieve consistency in handling analytical data derived from the cores. Samples removed from the cores are designated by distance measured in centimeters from the top of the section to the top and bottom of each sample removed from that section. A full identification number for a sample consists of the following information: leg, site, hole, core number, core type, section number, piece number (for hard rock), and interval in centimeters measured from the top of section. For example, a sample identification of “203-1243B-2R-1, 80–85 cm,” would be interpreted as representing a sample removed from the interval between 80 and 85 cm below the top of Section 1. Core 2R designates that this core was taken with the rotary core barrel (RCB) from Hole 1243B drilled during Leg 203 (Fig. F1).

All ODP core identifiers indicate core type. The following abbreviations are used:

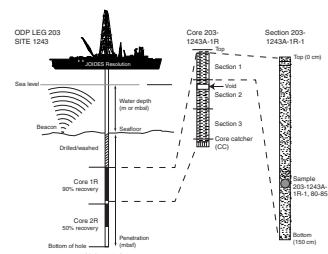
- H = hydraulic piston core (also referred to as advanced hydraulic piston corer or advanced piston corer [APC]).
- X = extended core barrel (XCB).
- R = RCB.
- N = motor-driven core barrel.
- M = miscellaneous material.

### **Core Handling**

As soon as a core is retrieved on deck, it goes through a sequence of processing steps. Because only one, short, extremely disturbed sediment core was recovered during Leg 203, no CC or interstitial water (IW) samples were taken.

Each section of both sediment and igneous rock cores is sealed at the top and bottom by gluing on color-coded plastic caps (blue to identify the top of a section and clear for the bottom). The caps are usually attached to the liner by coating the end liner and the inside rim of the cap with acetone. Then the caps are taped to the liners. The core sections are then carried into the laboratory where the individual sections are again labeled using an engraver to mark permanently the full designation of the section. The length of the core in each section is measured to the nearest centimeter; this information is logged into the ODP Janus database.

**F1.** Illustration of numbering of cores, p. 32.



After a core has equilibrated to room temperature, which usually takes ~1–3 hr, physical properties measurements are made on the whole-round core material (see “[Physical Properties](#),” p. 15)

Cores of soft material are split lengthwise into working and archive halves. The softer cores are split with a wire or saw depending on the degree of induration. Harder cores are split with a band saw or diamond saw. The wire-cut cores are split from bottom to top, so investigators should be aware that older material could have been transported up the core on the split face of each section.

Igneous rock cores are handled differently from sediment cores. Once on deck, the CC sample is placed at the bottom of the core liner and total core recovery is calculated by pushing the rock pieces together and measuring to the nearest centimeter. The core then is cut into 1.5-m-long sections and transferred into the laboratory.

The contents of each section are transferred into 1.5-m-long sections of split core liner, where the bottoms of oriented pieces (i.e., pieces that clearly could not have rotated top to bottom about a horizontal axis in the liner) are marked with a red wax pencil. This is done to ensure that the orientation is not lost during the splitting and labeling processes. Important primary features of the cores also are recorded at this time. A plastic spacer is used to separate individual pieces and/or reconstructed contiguous groups of pieces in the core liner. These spacers may represent a substantial interval of no recovery. The length of each section is then recorded and entered into the database as the curated length. The curated length will commonly differ by a few centimeters from that measured on the catwalk. Each piece of core is then split into archive and working halves, with the positions of spacers maintained for both halves. Each piece is numbered sequentially from the top of each section, beginning with number one; reconstructed groups of pieces are assigned the same number but are lettered consecutively. Pieces are labeled only on the outer cylindrical surfaces of the core. If the piece is oriented, an arrow is added to the label, pointing to the top of the section. Because pieces are free to turn about a vertical axis during drilling, determination of azimuthal orientation during Leg 203 was possible only by using paleomagnetic measurements or by matching digital images made of the exterior of the core with Formation MicroScanner (FMS) images of the borehole wall.

### **All Cores**

For all cores, the archive half is described visually (see “[Core Descriptions](#),” p. 4). Smear slides are made from small amounts of sediment samples taken from the archive half.

Digital images of the archive halves are made using the GEOTEK X-Y imaging system, with its digital camera, light source, x- and y-axis stepper motors, core racks, and appropriate software. In the ODP configuration for camera height and imaging length (180 cm) and width (9 cm), the linescan images have a resolution of 100 pixels per centimeter.

Most archive sections are run through the archive multisensor track (AMST) for color reflectance spectroscopy measurements and susceptibility measurements, with a point susceptibility meter. Color reflectance is determined using a Minolta CM-2002 spectrophotometer. Measurements are made in thirty-one 10-nm-wide bands of the visible spectrum (400–700 nm) on the archive half of each core section. Spectrophotometer readings were taken after covering the surface of each core section with clear plastic film. Calibration for the color scanner did

not include a correction for the plastic film because the effect is minor, even with very brightly colored lithologies. The area measured is a circle 8 mm in diameter, and the spectrophotometer integrates the sensed color over this area. Measurements were made every 5 cm along each core section. The AMST was not programmed to avoid taking measurements in intervals with a depressed core surface or in disturbed areas of core with drilling slurry or biscuits. The color data are a part of the ODP database. Additional information about measurement and interpretation of spectral data with the Minolta spectrophotometer can be found in Balsam et al. (1997, 1998) and Balsam and Damuth (2000).

Finally, the archive half is run through the cryogenic magnetometer for magnetic remanence measurements, then photographed using black-and-white and color film. Close-up photographs (color and monochrome) are taken of particular features for illustrations in the summary of each site, as requested by individual scientists.

The working half of the core is sampled for both shipboard and shore-based laboratory study. Each extracted sample is logged into the sampling computer database and referenced by the location and name of the investigator receiving the sample. Records of all removed samples are kept by the curator at ODP. The extracted samples are sealed in plastic vials, cubes, or bags and labeled. Samples are routinely taken for shipboard physical properties, paleomagnetic, thin section, and geochemistry analyses as described in the sections below.

Following the initial scientific measurements and sampling, both halves of igneous cores are shrink-wrapped in plastic to prevent rock pieces from vibrating out of sequence during transit. The working and archive halves of sedimentary and igneous cores are then put into labeled plastic tubes, sealed, and transferred to cold-storage space on board the drilling vessel. At the end of Leg 203, the cores were transferred in refrigerated containers from the ship to cold storage at the ODP Gulf Coast Repository at Texas A&M University in College Station, Texas.

## **CORE DESCRIPTIONS**

Core description forms provide a summary of data obtained during shipboard analysis of the sediments. Detailed observation of each core section of sediments was recorded initially by hand on standard ODP visual core description (VCD) forms. The sediment VCD was then transcribed using AppleCORE software. Separate VCDs were custom designed in Adobe Illustrator for the basalts (hard rock VCD [HR-VCD]). The basalt cores were described on hard copy HR-VCDs. These were then entered into the computer using Adobe Illustrator. The computerized versions of the VCDs are renamed electronic VCDs (eVCDs) or electronic HR-VCDs (eHR-VCDs).

The overall procedures used here are similar to those developed by the scientific parties during previous ODP legs. The emphasis of our on-board studies was to produce an integrated picture of the various units recorded from the hole. Note that depths recorded for recovered cores may differ from true depths owing to curation protocol, in which the top of a core is placed at the top of the cored interval. When recovery is <100%, the depths attached to the recovered cores will be shallower or equal to the true depths because all that is actually known is that the core came from within the cored interval.

## Sediments

### Sediment Classification

Recovery of sediment during Leg 203 was modest, so our classification only considers pelagic sediment and limestone. Sedimentary terms and concepts in this chapter and in the site chapter are those in common usage (e.g., Boggs, 1995), except as otherwise referenced. Because Site 1243 is closely adjacent to Site 852, which was drilled during Leg 138, we have used the sediment classification scheme used by the Leg 138 Shipboard Scientific Party (Mayer, Pias, Janecek, et al., 1992) that is in common use for biogenic pelagic sediments that fell into the borehole. Lithologic names of the ODP sediment classification scheme (Mazzullo et al., 1988) are more appropriate for detrital and hemipelagic sediments. For Legs 138 and 203, sediment names consist of a principal name selected from the appropriate corner of the foraminifera-nannofossil-diatom-radiolarian tetrahedron (e.g., foraminifer ooze) and a modifier that precedes the principal name of components >10%, given in order of increasing abundance (e.g., diatom nannofossil foraminifer ooze). None of the sediments from Site 1243 had nonbiogenic components >10%, which might have resulted in a modified name for the ooze. Composition was estimated from smear slides.

The recovered limestone was classified according to its composition and texture (Folk, 1962) and its texture when deposited (Dunham, 1962). Composition and texture were estimated from thin section. Specifically, with 10%–50% of the rock composed of allochemical grains (formed of calcite and moved, not formed in place), the adjective “sparse” is used. The name also includes any significant biogenic grains, which, in this case, are foraminifer microfossils. Abbreviations of the allochemical grains enter the rock name, in this case subequal amounts of peloidal and biogenic allochemicals. As more than two-thirds of the intergranular material is lime-mud matrix rather than sparry calcite cement, the rock name includes the term microcrystalline calcite (micrite). Thus, according to Folk (1962), the limestone is a sparse foraminiferal pelbiomicrite. At the time of deposition, its texture was that of grains of coarse silt and larger sizes (>0.03 mm), comprising >10% of the rock and supported by a muddy matrix. Thus, according to Dunham (1962), the limestone is a wackestone.

### AppleCORE Sheets

The electronic descriptions for sediments were created using AppleCORE (v. 8.1m) software, which generates a simplified annotated graphic for each core (Fig. F2). Columns on the AppleCORE sheets include depth, core section, graphic lithology, bioturbation, sedimentary structures and other lithologic and fossil features, core disturbance, sample type, and description of the core. Features related to the cores are either plotted on the graphic lithology near the interval where they are present or included in the “Description” column. The columns on the barrel sheets appropriate to Leg 203 include graphic lithology, where sediment lithologies are represented by patterns, core disturbance, shipboard samples, and description, as discussed below.

F2. AppleCORE barrel sheet, p. 33.

Site 1243 Hole B Core 1R Cored 102.0-108.6 mbsf							
DEPTH (m)	CORE SECTION	GRAPHIC LITHOLOGY	BIOTURBATION	SEDIMENTARY STRUCTURES	CORE DISTURBANCE	SAMPLE TYPE	DESCRIPTION
102.0							
103.0							
104.0							
105.0							
106.0							
107.0							
108.6							

Note: Core consists of five individual core pieces in a barrel of more disturbed mud. The core formed on deck as large clasts of mudstone or sandy silt. The logs represent the original position of the core pieces and the core was reassembled at the end of the haul. Lumps and their results are changed and shown in color.

## **Core Disturbance**

Deformation and disturbance of sediment that resulted from the coring process are illustrated in the “Disturbance” column. Intensity of disturbance is not denoted by a symbol but is described in the “Description” column. The pelagic oozes recovered at Site 1243 were highly disturbed from having sloughed into the borehole, followed by the coring and recovery process. Bedding cannot be seen, and original stratigraphic position cannot be determined.

## **Shipboard Samples**

Sample material taken for shipboard sedimentological and chemical analyses consists of smear slide, thin section, X-ray diffraction (XRD), carbon-carbonate, and inductively coupled plasma-atomic emission spectroscopy (ICP-AES) samples. The sample type and the location in the section are noted in the “Sample” column.

## **Visual Description**

The written description for each core, located in the “Description” column on the AppleCORE sheets, contains a brief overview of both major and minor lithologies present, color gradation, grain-size gradation, location of samples in the section, and intensity of core disturbance.

## **Color**

Sediment and hard rock color was determined visually by comparison with standard Munsell color charts (Munsell Color Co., 1994; Rock-Color Chart Committee, 1991) and is reported in general terms in the “Description” column and in more detail on the original VCD sheets.

## **Smear Slides**

Grain size and composition of sediments were determined using smear slides. These were prepared according to the procedures described in the handbook for shipboard sedimentologists (Mazullo et al., 1988). Identification in terms of general components was undertaken in accordance with Rothwell (1989). For semiquantitative visual estimation of sediment textures and determination of major components, we used the Comparison Chart for Visual Percentage Estimation determined by Terry and Chilingar (1955), with the percentages corrected to compensate for the degree of dispersion of the grains in the smear slide. Quantitative estimates of grain size and of the main components are made to the nearest 5% on the smear slide worksheet and carried forward to the smear slide tables (see the “[Core Descriptions](#)” contents list). Care was taken to correct for the area taken on the smear slide by the mounting medium.

## **Thin Sections of Sediments**

We examined thin sections from the cored intervals to complement and refine the hand specimen observations. Tables summarizing data from thin sections and smear slides are included this volume (see the “[Core Descriptions](#)” contents list). These tables include information about the locations of samples in the core and an estimate of the abun-

dance, grain sizes, and other textural properties of the allochemical grains, micrite matrix, orthochemical crystals, and pores. No sedimentary structures were seen, except for some small burrows.

## Igneous Rocks

### Core Curation and Shipboard Sampling

In order to describe important mineralogic and structural features in both the archive and working halves, we examined core sections containing igneous rocks prior to cutting with a diamond-impregnated saw.

After the core was split, lithologic descriptions were made of the archive half, and the working half was sampled for shipboard physical properties measurements (see “Physical Properties,” p. 15), magnetic studies (see “Paleomagnetism,” p. 13), thin sections, and ICP-AES analyses. The archive half was described on the eHR-VCD form and photographed.

### Electronic Hard Rock Visual Core Descriptions

We used eHR-VCD forms (Fig. F3) to document each section of the igneous rock cores. The eHR-VCD columns, from the left, are “Piece Number,” “Graphic Representation,” “Orientation,” “Shipboard Studies,” “Lithologic Unit,” “Phenocrysts (%),” “Grain Size,” “Vesicularity,” and “Degree of Alteration and Veins.” The Graphic Representation column on the form represents the archive half. A horizontal line across the entire width of the column denotes a plastic spacer. Oriented pieces are indicated on the form by an upward-pointing arrow to the right of the piece. The key to the symbols, colors, and other notations used on the eHR-VCDs are reported in Figure F4. As on the AppleCORE sediment descriptions, locations of samples selected for shipboard studies are indicated in the column headed Shipboard Studies with the following notation: XRD analysis, ICP-AES, petrographic thin section, physical properties measurements, and paleomagnetic measurements.

### Lithologic Units

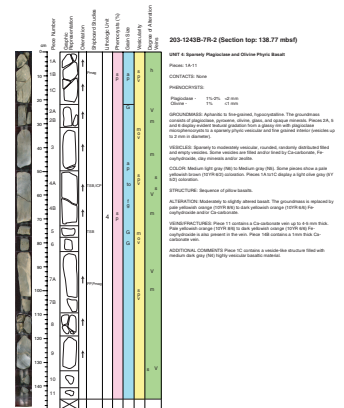
We subdivided the core into consecutively numbered lithologic units (denoted in the “Lithologic Unit” column on the eHR-VCD) on the basis of changes in color, structure, brecciation, grain size, vesicle abundance, mineral presence and abundance, and the presence of sedimentary interbeds.

### Phenocrysts

The “Phenocryst” (in percent) column is used to represent a visual estimation of abundance and variation of phenocrysts throughout the core section using the following notations:

- a = aphyric (phenocryst content is <1%).
- sp = sparsely phyrlic (phenocryst content is 1%–2%).
- mp = moderately phyrlic (phenocryst content is >2%–10%).
- hp = highly phyrlic (phenocryst content is >10%).

F3. A Leg 203 eHR-VCD, p. 34.



F4. Key to the eHR-VCD, p. 35.

Igneous texture/structures definitions and abbreviations													
Phenocryst	<table border="0"> <tr> <td>a</td> <td>sp</td> <td>mp</td> <td>hp</td> </tr> <tr> <td>Aphyric (&lt;1%)</td> <td>Sparsely phyrlic (1%-2%)</td> <td>Moderately phyrlic (&gt;2%-10%)</td> <td>Highly phyrlic (&gt;10%)</td> </tr> </table>	a	sp	mp	hp	Aphyric (<1%)	Sparsely phyrlic (1%-2%)	Moderately phyrlic (>2%-10%)	Highly phyrlic (>10%)				
a	sp	mp	hp										
Aphyric (<1%)	Sparsely phyrlic (1%-2%)	Moderately phyrlic (>2%-10%)	Highly phyrlic (>10%)										
Grain size	<table border="0"> <tr> <td>G</td> <td>S</td> <td>F</td> <td>M</td> </tr> <tr> <td>Glass</td> <td>Aphanitic (&lt;1 mm)</td> <td>Fine grained (&lt;2 mm)</td> <td>Medium grained (&gt;2 mm)</td> </tr> </table>	G	S	F	M	Glass	Aphanitic (<1 mm)	Fine grained (<2 mm)	Medium grained (>2 mm)				
G	S	F	M										
Glass	Aphanitic (<1 mm)	Fine grained (<2 mm)	Medium grained (>2 mm)										
Vesicularity	<table border="0"> <tr> <td>n</td> <td>s</td> <td>m</td> <td>h</td> </tr> <tr> <td>Nonvesicular (&lt;1%)</td> <td>Sparsely vesicular (1%-2%)</td> <td>Moderately vesicular (&gt;2%-10%)</td> <td>Highly vesicular (&gt;10%)</td> </tr> </table>	n	s	m	h	Nonvesicular (<1%)	Sparsely vesicular (1%-2%)	Moderately vesicular (>2%-10%)	Highly vesicular (>10%)				
n	s	m	h										
Nonvesicular (<1%)	Sparsely vesicular (1%-2%)	Moderately vesicular (>2%-10%)	Highly vesicular (>10%)										
Degree of alteration	<table border="0"> <tr> <td>f</td> <td>s</td> <td>m</td> <td>h</td> <td>vh</td> <td>c</td> </tr> <tr> <td>Unaltered (&lt;1%)</td> <td>Slight (&gt;1%-5%)</td> <td>Moderate (&gt;5%-10%)</td> <td>High (&gt;10%-20%)</td> <td>Very high (&gt;20%-50%)</td> <td>Complete (&gt;50%-100%)</td> </tr> </table>	f	s	m	h	vh	c	Unaltered (<1%)	Slight (>1%-5%)	Moderate (>5%-10%)	High (>10%-20%)	Very high (>20%-50%)	Complete (>50%-100%)
f	s	m	h	vh	c								
Unaltered (<1%)	Slight (>1%-5%)	Moderate (>5%-10%)	High (>10%-20%)	Very high (>20%-50%)	Complete (>50%-100%)								
Veins	<table border="0"> <tr> <td>V</td> <td>Veins present</td> </tr> </table>	V	Veins present										
V	Veins present												

### **Grain Size**

The "Grain Size" column shows, schematically, the nature of the groundmass and the presence of glass. The following notations were used:

- G = glass.
- ap = aphanitic (<1 mm).
- fg = fine grained (1–2 mm).
- mg = medium grained (>2–5 mm).
- cg = coarse grained (>5 mm).

### **Vesicularity**

The "Vesicularity" column describes the vesicle content and uses the following notations:

- nv = nonvesicular (vesicle content is <1%).
- spv = sparsely vesicular (vesicle content is 1%–5%).
- mov = moderately vesicular (vesicle content is >5%–20%).
- hiv = highly vesicular (vesicle content is >20%).

### **Degree of Alteration and Veins**

The "Degree of Alteration" and "Veins" column estimates the degree of alteration and denotes the presence of veins with the letter "V." The alteration was described using the following notations:

- f = unaltered (alteration products form <2% of the rock).
- s = slight (alteration products form 2%–10% of the rock).
- m = moderate (alteration products form >10%–40% of the rock).
- h = high (alteration products form >40%–80% of the rock).
- vh = very high (alteration products form >80%–95% of the rock).
- c = complete (alteration products form >95%–100% of the rock).

### **Written Descriptions**

Written core descriptions accompany the schematic representation of the core sections. These include "Leg, Site, and Hole" and "Unit Number and Rock Name," in addition to the columns "Pieces," "Contacts," "Phenocrysts," "Groundmass," "Vesicles," "Color," "Structure," "Alteration," "Veins/Fractures," and "Additional Comments."

### **Leg, Site, and Hole**

The leg, site, hole, core type, and section number (e.g., 203-1243R-3R-2), as well as the top of the core section measured in mbsf, are located at the top.

### **Unit Number and Rock Name**

The unit number (consecutive downhole) and the rock name are located next to the unit. We assigned provisional rock names on the basis of hand specimen observation (hand lens and binocular microscope) and later checked these assignments by examining thin section and ICP-AES analyses. Porphyritic rocks were named by phenocryst type;



the term “phenocryst” was used for a crystal that was significantly, typically five times, larger than the average size of the groundmass crystals and generally euhedral to subhedral in shape. This nomenclature is sensitive to changes in the groundmass grain size; for example, a single cooling unit could have a moderately phyric aphanitic margin and an aphyric fine-grained interior without any change in the distribution or size of the early formed crystals. In order to avoid the problem of describing pillow margins as phyric and cogenetic pillow interiors as aphyric, we based our terminology on the aphanitic margins of cooling units. Thus, if aphanitic pillow margins were sparsely olivine phyric basalt, we described the fine-grained interiors using the same name, even though the euhedral olivine phenocrysts in the pillow interiors were similar in size to groundmass plagioclase laths. Phenocryst phases, in order of decreasing abundance, were included in the rock name. Thus, a “highly olivine plagioclase phyric basalt” contains >10% (by volume) phenocrysts, the dominant phenocryst being olivine, with lesser amounts of plagioclase. As long as the total content >1%, the minerals named include all of the phenocryst phases that are present in the rock.

### **Contacts**

The “Contacts” column includes contact relations and unit boundaries. After we made lithologic descriptions, we attempted to integrate the observations in order to define unit boundaries. The boundaries commonly reflect physical changes in the core (e.g., pillowed vs. massive) that were also observed in the physical properties and downhole measurements. Intervals of sediment and/or breccia, changes in vesicularity, glass, chilled margins, alteration, volume fraction, and type of matrix also define lithologic contacts. Where possible, whole-rock chemical analyses by ICP-AES were used to investigate chemical differences between units.

### **Phenocrysts**

The “Phenocryst” column describes the types of minerals visible with a hand lens or a binocular microscope and their distribution within the unit and for each phase its abundance (in volume percent), size range (in millimeters), shape, and degree of alteration, with further comments if appropriate.

### **Groundmass**

The “Groundmass” column includes texture and grain size: glassy, aphanitic (<1 mm), fine grained (1–2 mm), medium grained (>2–5 mm), or coarse grained (>5 mm). Changes in grain size and proportions of crystals and glass within units were also noted.

### **Vesicles**

The “Vesicles” column records vesicle abundance (visual estimates of the volume fraction of vesicles were supplemented by observations using a binocular microscope), size, shape (sphericity and angularity), whether the vesicles are empty or filled, and the nature of the filling.

## Color

The “Color” column includes a color name and code (for the dry rock surface) according to the standard rock color charts (Munsell Color Co., 1994).

## Structure

The “Structure” column describes fractures that are lined with various alteration minerals, which may have adjacent zones of altered rock or alteration halos. In addition, this entry refers to whether the unit is massive, pillowed, or brecciated. Pillowed sequences were inferred using the presence of glassy margins, groundmass grain-size variations, and vesicle-rich bands. A section was described as massive if there was no evidence for pillows, even though it may be part of a pillowed sequence.

## Alteration

The “Alteration” column describes the degree of alteration as unaltered (<2% by volume of alteration products), slight (2%–10%), moderate (>10%–40%), high (>40%–80%), very high (>80%–95%), or complete (>95%–100%). Changes in alteration through a section or a unit were noted, in addition to the type of alteration material.

## Veins/Fractures

The “Veins/Fractures” column describes the abundance, width, and mineral linings and fillings of the veins and fractures.

## Additional Comments

The “Additional Comments” column describes any general descriptions of the unit that were not included under another column.

## Thin Section Descriptions

We examined thin sections in order to confirm the VCDs and to define the textures and relationships among the various constituents of the units. Thin section descriptions also helped to define the secondary alteration mineralogy. In general, the same terminology was used for thin section descriptions, as for the VCDs. The percentages of individual phenocryst, groundmass, and alteration phases were estimated visually, and textural descriptions are reported in “[Site 1243 Thin Sections](#).” Mineral identifications were made using standard optical mineralogical techniques. The textural terms used are defined by MacKenzie et al. (1982). Thin section descriptions also include thumbnail copies of photomicrographs.

## Alteration and Vein Logs

Alteration and vein core description logs were tabulated to provide a consistent characterization of the rocks and to quantify the different alteration types. Descriptions are based mostly on hand specimen observations of wet cut surfaces; specific clay, zeolite, and carbonate minerals are not generally distinguished except where crystal morphology allows

unequivocal identification. We recorded the following information in the alteration and vein logs:

1. The alteration log was used to record bulk rock alteration and vesicle filling. Each entry records the igneous unit and identifiers for the core, section, and the depth below seafloor of the top of each piece and includes the following: visual estimates of the degree of alteration based on a scale ranging from zero (for unaltered samples) to five (for complete alteration), presence of secondary minerals such as Fe oxides and clays, visual estimates of vesicularity based on a scale ranging from zero (for nonvesicular samples) to three (for highly vesicular samples), and mineral fillings of vesicles.
2. The vein log was used to record the presence, location, apparent orientation, width, and mineral content of veins observed on the cut surface of the cores. Each entry records the igneous unit and identifiers for the core, section, piece, and the depth below seafloor of the top of each piece. For each vein, the depth, location of the top and bottom, vein width (in millimeters), apparent orientation, mineral fillings, and proportions of the feature are recorded. If a related alteration halo is present, its color, half width (in millimeters), alteration mineralogy, and proportions are described. A column for comments is included.

## **Geochemistry**

We performed chemical analyses of basalt during Leg 203 using ICP-AES. Selected representative samples of each unit were first cut with a diamond-impregnated saw blade and ground on a diamond wheel to remove surface contamination. Samples were washed in an ultrasonic bath containing methanol for ~10 min, followed by three consecutive ~10-min washes in an ultrasonic bath containing nanopure deionized water, and then dried for ~12 hr in an oven at 110°C. The cleaned whole-rock samples (~20 cm<sup>3</sup>) were reduced to fragments <1 cm in diameter by crushing them between two disks of Delrin plastic in a hydraulic press followed by grinding them for ~5 min in a Spex 8510 shatterbox with a tungsten carbide barrel. The sample powders were weighed on a Scientech balance and ignited to determine weight loss on ignition.

We weighed 100 ± 2 mg aliquots of the ignited whole-rock powders and mixed them with 400 ± 0.4 mg of lithium metaborate (LiBO<sub>2</sub>) flux that had been preweighed on shore. Standard rock powders and full procedural blanks were included with the unknowns for each sample run. All samples and standards were weighed on the Cahn Electrobalance. Weighing errors are conservatively estimated to be ±0.01 mg.

Mixtures of flux and rock powders were fused in Pt-Au crucibles at 1050°C for 10–12 min in a Bead Sampler NT-2100. Ten microliters of 0.172-mM aqueous lithium bromide (LiBr) solution was added to the mixture before fusion as an antiwetting agent to prevent the cooled bead from sticking to the crucible. Cooled beads were transferred to 125-mL polypropylene bottles and dissolved in 50 mL of 2.3-M HNO<sub>3</sub> by shaking with a Burrell Wrist Action bottle shaker for 1 hr. After digestion of the glass bead, all of the solution was filtered to 0.45 μM into a clean 60-mL widemouthed polypropylene bottle. Next, 2.5 mL of this solution was transferred to a plastic vial and diluted with 17.5-mL of 2.3 M of nitric acid (HNO<sub>3</sub>) to bring the total volume to 20 mL. The

solution-to-sample dilution factor for this procedure is ~4000. Dilutions were conducted using a Brinkman Dispensette (0.25 mL).

Major (Si, Ti, Al, Fe, Mn, Mg, Ca, Na, K, and P) and trace (Zr, Y, Sr, Ba, Ni, Cr, Sc, V, Nb, Co, Cu, and Zn) element concentrations of powder samples were determined with the JY2000 Ultrace ICP-AES. The JY2000 sequentially measures characteristic emission intensities (with wavelengths between ~100 and 800 nm). Murray et al. (2000) developed protocols for dissolution and ICP-AES analysis of rock powders. The hard rock analytical procedure was refined during Leg 197 (Shipboard Scientific Party, 2002). The elements analyzed, emission lines used, and the specific analytical conditions for each sample run during Leg 203 are provided in Table T1.

The JY2000 plasma was ignited 30 min before each run to allow the instrument to warm up and stabilize. After the warm-up period, a zero-order search was performed to check the mechanical zero of the diffraction grating. After the zero-order search, the mechanical step positions of emission lines were tuned by automatically searching with a 0.002-nm window across each emission peak using BCR-2 standard prepared in 2.3-M HNO<sub>3</sub>. The only exception is P, which was automatically searched by using a single-element standard. During the initial setup, an emission profile was collected for each peak, using BCR-2, to determine peak-to-background intensities and to set the locations of background points for each element. The JY2000 software uses these background locations to calculate the net intensity for each emission line. The photomultiplier voltage was optimized by automatically adjusting the gain for each element using the U.S. Geological Survey standard, BHVO-2 or BIR-1, with the highest concentration for that element. Before each run, a profile of BCR-2 was collected to assess the performance of the machine from day to day.

All ICP-AES data presented in the site chapter report were acquired using the Gaussian analytical mode of the Windows 5 JY2000 software. This mode fits a Gaussian curve to a variable number of points across a peak and then integrates to determine the area under the curve. Each unknown sample was run at least twice, nonsequentially, in all sample runs.

A typical ICP-AES run included the following:

1. A set of three certified rock standards (BHVO-2, BIR-1, and JB-1) (Table T2) run at the beginning, middle, and end of the sample run;
2. Up to eleven unknown samples;
3. A drift-correcting sample (BCR-2 standard) analyzed every third sample position and at the beginning and end of each run; and
4. Blank solutions run near the beginning, middle, and end of each run. A 2.3-M HNO<sub>3</sub> wash solution was run for a minimum of 90 s between each of the samples and standards.

Following each sample run, the raw intensities were transferred to a data file and data reduction was completed using a spreadsheet to ensure proper control over standardization and drift correction. Once transferred, intensities for all samples were corrected for the full procedural blank. A drift correction was then applied to each element by linear interpolation between drift-monitoring solutions run before and after a particular batch of samples. The interpolation was calculated using the lever rule. Following blank subtraction and drift correction, concentrations for each sample were calculated from the average intensity per unit

---

T1. ICP-AES parameters, p. 52.

---

---

T2. Rock standard, p. 53.

---

concentration for the standards BHVO-2, BIR-1, and JB-1, which were analyzed twice during the run.

Estimates of accuracy and precision for major and trace element analyses were based on replicate analyses of BHVO-2, BIR-1, and JB-1, the results of which are presented in Table T2. In general, run-to-run relative precision by ICP-AES was better than 2% for the major elements. Run-to-run relative precision for trace elements was within 5%. Exceptions typically occurred when the element in question was near the detection limit of the instrument (see Table T1 for instrument detection limits).

## **PALEOMAGNETISM**

Paleomagnetic investigations conducted on board the *JOIDES Resolution* during Leg 203 consisted of routine measurements of natural remanent magnetization (NRM) and of magnetic susceptibility (MS) of igneous rocks. NRM was measured on all archive split cores of recovered rocks and on discrete samples of basement rocks taken from the working halves. Stepwise alternating-field (AF) demagnetization was carried out on all archive-half cores and on some discrete samples in an attempt to isolate stable components of remanence. A few discrete samples were thermally demagnetized in an effort to obtain their primary remanent magnetization and identify magnetic carriers. MS was measured for whole cores, archive-half core sections, and, in a few cases, discrete samples. To investigate rock magnetic properties, we also conducted isothermal remanent magnetization (IRM) experiments and thermal demagnetization of the IRM on some of the discrete samples. Magnetic properties were compared with lithologic units.

### **Laboratory Instruments**

The remanence of archive-half sections and oriented discrete samples from working-half sections was measured using a 2-G Enterprises pass-through cryogenic direct-current superconducting quantum interference device (DC-SQUID) rock magnetometer (model 760R). This pass-through cryogenic magnetometer is equipped with an in-line AF demagnetizer (2-G model 2G600) that allows for demagnetization of samples up to peak fields of 80 mT with a 200-Hz frequency. The practical limit on the resolution of natural remanence of core samples is imposed by the magnetization of the core liner itself (~0.01 mA/m). The magnetometer and AF demagnetizer are interfaced to a personal computer (PC) and are controlled by the 2G Long Core software by National Instruments. A Molspin spinner magnetometer was also available on the ship for measuring the remanence of discrete samples. For stepwise demagnetization of discrete samples, the laboratory contains an AF demagnetizer (model D-2000 by DTech Inc.) and a thermal demagnetizer (model TSD-1 by the Schonstedt Instrument Co.) capable of demagnetizing specimens to 200 mT and 700°C, respectively. An Analytical Services Company (ASC) model IM-10 impulse magnetizer (capable of pulsed fields from 0.02 to 1.35 T) was available for IRM acquisition studies of discrete samples.

MS was measured for all whole-core sections at 2-cm intervals using a susceptibility meter attached to the multisensor track (MST) (see “**Physical Properties**,” p. 15). The susceptibility values are stored in the Janus database as raw data in units of  $10^{-5}$  SI. The true SI volume of suscepti-

bilities should be multiplied by a correction factor to account for the volume of material that passed through the coils. The standard correction factor for ODP core is  $\sim 0.66$ . The MS of archive halves was routinely measured using the AMST (see “Core Descriptions,” p. 4) at 1-cm intervals. The measurements were recorded automatically by the AMST, which permits measurements only at evenly spaced intervals along each section of core. For the two types of susceptibility measurements (MST and AMST), the same type of MS meter (Bartington Instruments model MS2) was used but with a different sensor. The sensor for whole-core measurements (MS2C) has an 80-mm inner diameter, and the core passes through the sensor coil. A Geofyzika Brno Kappabridge KLY-2 MS meter was available for MS measurements of discrete samples.

To investigate rock magnetic characteristics of some of the discrete samples, IRM acquisition experiments were conducted. IRMs were imparted to the discrete samples by a direct current field generated in the ASC impulse magnetizer. The magnetization acquired by samples in progressively stronger applied fields, usually to saturation, was measured with the cryogenic magnetometer. We conducted thermal demagnetization of IRMs on a few samples to delineate the nature of magnetic remanence in the rocks.

### Core Orientation

The standard ODP core-orientation convention was applied for paleomagnetic work during Leg 203. This convention can be described as follows: the z-axis is downhole parallel to the core, the x-axis forms a line perpendicular to the split face of the core and is directed into the working half, and the x-axis is used as the reference “geomagnetic north” for the definition of magnetic declination values (Fig. F5). Discrete minicores were marked with an arrow in the negative z-direction (uphole) on the plane representing the split surface of the working half. The plane marked with the arrow is the y-z plane. Because only the RCB was used for drilling, we were unable to use the Tensor tool, which mounts on the APC core barrel to orient cores.

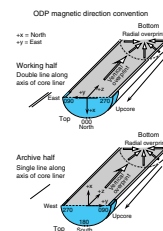
### Sampling Method

Oriented discrete samples were taken from the working half of each section (typically one or two per section for shipboard analyses) for on board pilot demagnetization studies. Cylindrical minicores ( $10.5 \text{ cm}^3$ ) were drilled from igneous rocks using a water-cooled nonmagnetic drill bit attached to a standard drill press. To minimize using core material for shipboard studies, most minicores were shared with the shipboard physical properties laboratory.

### Measurements

The NRM of the archive-half sections was analyzed on the cryogenic magnetometer at 1-cm intervals for igneous rocks when sufficiently long continuous pieces were available. To isolate the characteristic remanent magnetization (ChRM), archive halves were AF demagnetized up to a maximum peak field of 70 mT. Stepwise thermal demagnetization of up to  $580^\circ\text{C}$  was also applied to some discrete samples. IRM acquisition experiments were performed on some selected rocks in order to define their dominant magnetic mineralogy.

F5. Paleomagnetic coordinate system, p. 36.



## Analysis

The stability of remanence levels within the archive cores and the discrete samples were determined by both Zijderveld (1967) plots and equal-area stereographic projections. The ChRM of basalt samples was then obtained using principal component analysis (Kirschvink, 1980) on the results of the AF or thermal demagnetization.

Results from the remanent magnetization and low-field susceptibility measurements were compared with lithologic units and/or geologic structures based on sedimentary, petrologic, and structural features (see “Core Descriptions,” p. 4).

## PHYSICAL PROPERTIES

Shipboard measurements of physical properties are used to for characterizing lithologic units, for correlating cored material with downhole logging data, and for interpreting seismic reflection profiles.

After recovery, the cores were allowed to come to room temperature (22°–23°C), then thermal conductivity, bulk density, and MS were measured in a series of nondestructive tests. Additional measurements of *P*-wave velocity, bulk density, porosity, and water content were made on right circular cylinders of basalt cut from the split core. The same samples were used for paleomagnetic measurements.

### Nondestructive Tests

Four sets of measurements (MS, gamma ray attenuation [GRA] density, *P*-wave velocity, and natural gamma radiation [NGR]) can be made in sequence on whole-core sections on the MST. MST data are sampled at discrete intervals, with sampling intervals and count times chosen to optimize the resolution of the data in the time available to run each core section through the device. During Leg 203, no APC or XCB sediment cores were taken; consequently, only MS and GRA measurements were made on the basalt RCB cores

### Magnetic Susceptibility

The MST includes a Bartington susceptibility meter (model MS2C) that has an 8-cm loop and operates at 0.565 kHz with a field intensity of 80 A/m. Volume susceptibility, *k*, is a dimensionless measure of the degree to which material can be magnetized in an external magnetic field,

$$k = M/H,$$

where *M* is the magnetization induced in the material by an external field of strength *H*. MS is sensitive to variations of the type and content of magnetic grains in the sediment and, thus, is an indicator of compositional variations. During Leg 203, we sampled RCB basalt cores for 10 s at 2-cm intervals.

### Gamma Ray Attenuation Porosity Densitometer

GRA by Compton scattering is actually a measure of electron density. The method is useful for estimating the bulk densities of sediments and

crystalline rocks because the ratio  $Z/A$  of atomic number to atomic mass of elements that make up the common rock-forming minerals is essentially constant (see Blum, 1997). Porosity is estimated from GRA densities by using an assumed grain density.

The GRA densitometer measures the attenuation of a collimated beam of gamma rays from a  $^{137}\text{Ce}$  source as it passes through a sample of known thickness (Boyce, 1976). Having a well-known path length is critical to acquiring reliable GRA bulk densities. RCB basalt cores were sampled for 10 s at 2-cm intervals. Path-length corrections must be made before these data can be used.

### ***P*-Wave Velocity**

The *P*-wave logger was not used on RCB basalt cores.

### **Natural Gamma Radiation Detector**

The natural gamma radiation detector was not used on the RCB basalt cores recovered during Leg 203.

### **Thermal Conductivity**

Thermal conductivity is measured by transient heating of a material with a known heating power generated from a source of known geometry and then measuring the temperature change with time, using the TK04 system described by Blum (1997). Thermal conductivity profiles of sediments and rock sections are used, with temperature measurements, to estimate heat flow. The needle probe method is used in full-space (von Herzen and Maxwell, 1959) configuration for soft sediments and in half-space mode (Vacquier, 1985) for lithified sediment and hard rock samples. The thermal conductivity of hard materials is measured on split-core pieces (working half). Measurements were made at an interval of one per core.

### ***P*-Wave Velocity**

The PWS3 (Hamilton Frame) was used to measure velocities in discrete samples (minicores) of basalt. The PWS3 is a modified and updated version of the classic Hamilton Frame velocimeter, in which one transducer is fixed and the other is mounted on a screw. The PWS3 is mounted vertically to measure velocities in the  $x$ -direction (perpendicular to the core axis) by placing the sample on the lower transducer and bringing the upper transducer into direct contact with the upper surface. To improve the coupling (i.e., the impedance match) between the transducer and the sample, water is commonly applied to the top and bottom of the sample and transducer heads. Traveltimes are picked manually or automatically by the threshold method, and the transducer separation is recorded by a digital caliper. During Leg 203, we measured *P*-wave velocities in discrete samples of basalt recovered from basement.

### **Moisture and Density**

The minicores of basalt used for the velocity measurements were also used to estimate bulk density, grain density, and porosity from the volumes and wet and dry weights of the samples. Volumes were calculated



from the dimensions of the samples. Sample mass is determined to a precision of  $\pm 0.001$  g using two Scientech electronic balances. The balances are equipped with a computer averaging system that compensates for the motion of the ship. The sample mass on one balance is counterbalanced by a known mass on the adjacent balance. Sample volumes are determined using a five-cell Quantachrome Penta-Pycnometer helium-displacement pycnometer with a nominal precision of  $\pm 0.01$  cm<sup>3</sup>. Sample volumes are measured at least three times and then averaged. A standard reference sphere is run sequentially in each of the five operating cells to maintain calibration. The cell volume is recalibrated if the measured volume of the standard is not within 0.02 cm<sup>3</sup> of the known volume of the standard. Dry weight and volume measurements were made after the samples were oven dried at  $105 \pm 5^\circ\text{C}$  for 24 hr and allowed to cool in a desiccator. A potential problem with this drying temperature is that chemically bound water in some clay minerals can be lost in addition to IW.

### **Water Content**

Water content, as a fraction of total mass or as a ratio of water mass to solid mass, is determined by standard methods of the American Society for Testing and Materials (ASTM) designation (D) 2216 (ASTM, 1989). The total water-saturated mass ( $M_t$ ) and dry mass ( $M_d$ ) are measured using the electronic balance as described above, and the difference is the uncorrected water mass. Measured wet and dry masses are corrected for salt assuming a pore water salinity ( $r$ ) of 0.35% (Boyce, 1976). The wet and dry water contents ( $W_d$  and  $W_w$ ) are given by

$$W_d (\% \text{ dry mass}) = [(M_t - M_d)/(M_d - rM_t)] \times 100 \text{ and}$$

$$W_w (\% \text{ wet mass}) = [(M_t - M_d)/[(1-r)M_t]] \times 100,$$

where  $M_t$  is the mass of the saturated sample.

### **Bulk Density**

Bulk density ( $\rho_b$ ) is the density of the saturated sample

$$\rho_b = M_t/V_t,$$

where  $V_t$  is the total sample volume, which is estimated from the dimensions of the minicores or from the volume of the dry sample ( $V_d$ ) and the volume of the pore fluid ( $V_w$ ) (see below):

$$V_t = V_d + V_w.$$

### **Grain Density**

Grain density ( $\rho_g$ ) is determined from the dry mass and dry volume measurements. Both mass and volume must be corrected for the salt content of the pore fluid,

$$\rho_g = (M_d - M_s)/(V_d - [M_s/\rho_s]),$$

where  $M_d$  is the mass of salt in the pore fluid and  $\rho_s$  is the density of salt (2.257 g/cm<sup>3</sup>).

Since  $M_s = rM_w$ ,  $M_w$  the salt-corrected mass of the seawater, is given by,

$$M_w = (M_t - M_d)/(1-r).$$

The volume of pore water is

$$V_w = (M_t - M_d)/(1-r)\rho_w.$$

### **Porosity**

Porosity ( $f$ ) is the ratio of pore water volume to total volume and can be calculated from fluid density, grain density, and bulk density of the material,

$$f = [(\rho_g - \rho_b)/(\rho_g - \rho_w)] \times 100,$$

where  $\rho_g$  is the grain density,  $\rho_b$  is the bulk density, and  $\rho_w$  is the density of the pore fluid, which is assumed to be seawater.

### **Dry Density**

The dry density ( $\rho_d$ ) is the ratio of the dry mass ( $M_d$ ) to the total volume ( $V_t$ ). The dry density is calculated from the corrected water content ( $W_d$ ) and porosity ( $f$ ),

$$\rho_d = (f/W_d) \times \rho_w.$$

## **WIRELINE LOGGING**

Downhole logs represent continuous measurements of the drilled formations as a function of depth. The advantage of downhole logging is the ability to record, concurrently, petrophysical as well as structural information of several properties. Operating on an intermediate scale between core measurements and borehole geophysics, downhole logs are characterized by fast data acquisition over large depth ranges under in situ conditions. During Leg 203, the Lamont-Doherty Earth Observatory Borehole Research Group (LDEO-BRG) performed open-hole measurements using the two ODP standard tool strings (triple combination [triple combo] and FMS-sonic) and two specialty tools (Well Seismic Tool [WST] and cement bond tool [CBT]). The first three of the above-mentioned tools were deployed in Hole 1243B, whereas the last tool was deployed in Hole 1243A. Additional data for borehole deviation in Hole 1234A were gathered by the General Purpose Inclinator Tool (GPIT) of the FMS-sonic tool string. Generally, all measurements were performed while the tools were pulled upward. That is, the tools were lowered down the hole on a heave-compensated electrical wireline and then pulled up at constant speed of ~250–300 m/hr. The sampling interval of log data ranges from 15 cm for standard tools to 2.5 mm for high-resolution tools, such as the FMS.

The main target of downhole measurements during Leg 203 is the reconstruction of the drilled lithologic units. This includes a reorienta-

tion of core data on the basis of high-resolution images provided by the FMS. Measurements of porosity, *P*-wave velocity, and density allow the depiction of zones of weakness, which may subsequently influence borehole stability. A quick-view estimation of these logging data provides depth ranges, and, to a certain extent, lateral extension of these zones. Measurements of gamma ray activity, including its spectral proportions of potassium, thorium, and uranium, address issues concerning evolution of alteration assemblages within the drilled basaltic sequences. The WST provides a check shot vertical seismic profile (VSP) survey to estimate a depth-traveltime plot and to calibrate the sonic log.

### Tool Strings and Logging Operations

The following tool strings used during Leg 203 were deployed in five logging runs. Runs one through three were performed in Hole 1243B, and runs four and five covered Hole 1243A.

Run one: the triple combo (resistivity, density, and porosity) tool string (Fig. F6) consists of the Accelerator Porosity Sonde (APS), the Hostile Environment Natural Gamma Ray Sonde (HNGS), the Hostile Environment Litho-Density Tool (HLDT), and the Dual Induction Tool (DIT). The Lamont-Doherty Temperature/Acceleration/Pressure tool (TAP) is attached to the bottom of the tool string.

Run two: the FMS-sonic tool string (Figs. F6, F7) consists of the FMS, the GPIT, a Dipole Sonic Imager (DSI), and the Natural Gamma Ray Spectrometry Tool (NGT). This last tool is included between the DSI and the FMS and is used to identify lithologic markers, providing a common reference for correlation and depth between the first two logging runs.

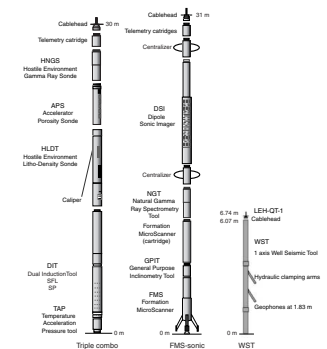
Run three: The deployment of the single-axis WST (Fig. F6) also required the operation of a generator-injector gun (GI) as a seismic source (Fig. F8).

Run four: the GPIT device is commonly used as an inclinometer device with the FMS tool (see above). The measurements made by the geomagnetic field sensors in the tool may be affected by the magnetization of the casing and drill pipe. Thus, the tool only provided accurate measurements for hole deviation as measured by its accelerometer (see below).

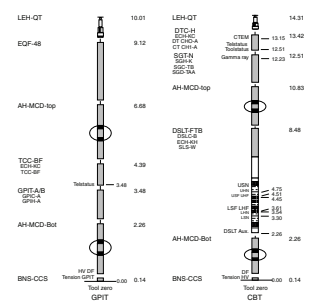
Run five: the CBT is used for measuring cement bond quality between the casing and surrounding formation. The CBT used in Hole 1243A was a short-spaced Digital Sonic Logging Tool (Fig. F7). It operates in a similar way as the DSI (see below) but with shorter spacings between the transducer-receiver pairs (3 and 5 ft), and it does not offer the dipole acquisition mode.

All tools were provided by Schlumberger, except the TAP, which was run by LDEO-BRG. Each tool string contains a telemetry cartridge providing communication along a 9000-m, double-armored, seven-conductor wireline with the Schlumberger Minimum Configuration Maxis (MCM) computer van on the drillship. The logging cable connects the MCM to the tool string through the logging winch and LDEO-BRG wireline heave compensator (WHC). The WHC is employed to minimize the effect of ship's heave on the tool position in the borehole. It re-

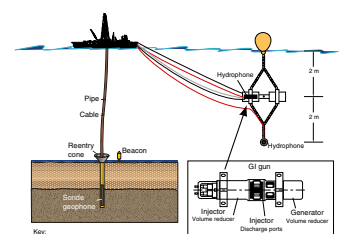
**F6. Tool strings used during Leg 203, p. 37.**



**F7. The GPIT and the CBT, p. 38.**



**F8. Schematic diagram of a gun configuration, p. 39.**



sponds to the ship's heave by hydraulically moving the compensator's heave to decouple the movement of the ship from the movement of the tool string in the borehole (Goldberg, 1990).

In preparation for logging, the borehole is usually flushed of debris by circulating viscous drilling fluid (sepiolite mud mixed with seawater; approximate density = 8.8 lb/gal or 1.11 g/cm<sup>3</sup>) through the drill pipe to the bottom of the hole. The bottom-hole assembly (BHA) is pulled up to a depth of between 50 and 100 mbsf, followed by a second run down to the bottom of the hole to repeat compensation of borehole irregularities. The hole is subsequently filled with additional sepiolite mud, and the pipe is raised to 50–70 mbsf, where it is kept to prevent hole collapse during logging.

The operating principles, applications, and approximate vertical resolution of the tools are summarized in Table T3. The principal data provided by the tools, their physical significance, and units of measure are listed in Table T4. More information on individual tools and their geological applications may be found in Desbrandes (1985), Ellis (1987), Goldberg (1997), Lovell et al. (1998), Rider (1996), Schlumberger (1989, 1994a, 1994b), Serra (1984, 1986, 1989), and the LDEO-BRG Wireline Logging Services Guide (Borehole Research Group, 1990). The basic principles of the tools and type of measurements are summarized below.

### Natural Radioactivity

Two spectral gamma ray tools were used to measure and classify natural radioactivity in the formation, the HNGS and the NGT. The NGT uses a sodium iodide (NaI) scintillation detector and five predefined energy windows to determine concentrations of K (in weight percent), Th (in parts per million), and U (in parts per million), the three elements whose isotopes dominate the natural radiation spectrum. The HNGS is similar to the NGT, but it uses two bismuth germanate (BGO) scintillation detectors and 256-window spectroscopy for a significantly improved tool precision. Gamma rays emitted by the formation pass the scintillator crystal in the tool and are converted to "light flashes" (Fig. F9). Subsequently, these flashes are converted to electrons through the photoelectric effect (PEF) and multiplied in the photomultiplier, producing distinctive energy peaks for the individual isotopes measured in millions of electron volts (MeV). The windows, described above, are designed to separate these energy peaks of the detected radioactive elements at 1.46 MeV for <sup>40</sup>K, 2.62 MeV for <sup>232</sup>Th, and 1.76 MeV for <sup>238</sup>U. Energies below 500 MeV are filtered out by the HNGS tool, eliminating sensitivity to bentonite or potassium chloride in the drilling mud and improving measurement accuracy. In contrast, NGT response is sensitive to borehole diameter and the weight and concentration of bentonite or potassium chloride present in the drilling mud. Corrections are routinely made for these effects during processing at LDEO-BRG.

For both tools, gamma ray values are measured in American Petroleum Institute units. These units are derived from the primary Schlumberger calibration test facility in Houston, Texas, where a calibration standard is used to normalize each tool.

### Density

Formation density is estimated from the density of electrons in the formation, which are measured with the Hostile Environment Litho-

---

T3. Wireline tool string measurements, p. 54.

---

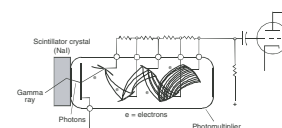


---

T4. Wireline logging tool acronyms and units, p. 55.

---

F9. Schematic drawing of a gamma ray tool, p. 40.



Density Sonde (HLDS). The sonde contains a radioactive cesium ( $^{137}\text{Cs}$ ) gamma ray source (622 keV) and far and near gamma ray detectors mounted on a shielded skid, which is pressed against the borehole wall by a hydraulically activated arm. Coupling between the tool and borehole wall is essential for good HLDS logging. Poor contact may occur when the borehole diameter is greater than the length of the caliper (e.g., for borehole diameters >48 cm), which results in underestimation of density values. Gamma rays emitted by the source experience Compton scattering (Fig. F10), which involves the transfer of energy from gamma rays to the electrons in the formation via elastic collision (further information is provided by Rider [1996] and Schlumberger [1989, 1994a, 1994b]). The number of scattered gamma rays that reach the detectors is directly related to the density of electrons in the formation, which is, in turn, related to bulk density. Porosity may also be derived from this bulk density if the matrix density is known.

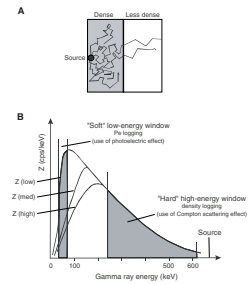
The HLDS also measures the PEF caused by absorption of low-energy gamma rays (Fig. F10). Photoelectric absorption occurs when gamma rays reach an energy level <150 keV after being repeatedly scattered by electrons in the formation. Photoelectric absorption is strongly dependent on the atomic number of the constituents of the formation. It varies according to the chemical composition and is essentially independent of porosity. For example, the PEF of pure calcite = 5.08 b/e<sup>-</sup>; illite = 3.03 b/e<sup>-</sup>; quartz = 1.81 b/e<sup>-</sup>; and kaolinite = 1.49 b/e<sup>-</sup>. In combination with the NGT log, PEF values can be used to identify different types of clay minerals. Hence, the PEF values can give an indication of the chemical composition of the rock. Coupling between the tool and borehole wall is essential for good HLDS logs. Poor contact results in underestimation of density values.

**Porosity**

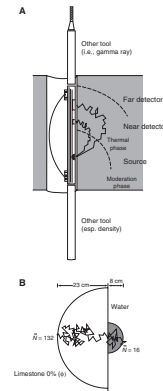
Formation porosity was measured with the APS. The sonde incorporates a minitron neutron generator, which produces fast neutrons (14.4 MeV), and five neutron detectors (four epithermal and one thermal) positioned at different intervals (spacing) from the minitron (Fig. F11). The tool is pressed against the borehole wall by a bow spring. Emitted neutrons are slowed by successive collisions with atomic nuclei in the formation (especially H), comparable to a billiard-ball effect. The amount of energy lost per collision depends on the relative mass of the nucleus with which the neutron collides. The greatest energy loss occurs when the neutron strikes a nucleus nearly equal to its own mass (such as H), which is mainly present in the pore water. After successive collisions, the speed of the thermal neutrons is so low that they are captured and absorbed by the formation's elements, thus, emitting a gamma ray in turn.

This provides the basis for two principal types of porosity measurements covered by contemporary neutron tools. Depending on the energy level, we can distinguish between (1) neutron-neutron and (2) neutron-gamma interactions. The former measures epithermal and thermal neutrons with an energy value of ~0.25 eV (Fig. F12). Neutrons with energy values lower than this are subject to diffusion and, finally, capturing by the elements in the formation (e.g., Cl, Si, and B). In turn, gamma rays are emitted by these elements, which can be measured by the second device (neutron-gamma). The APS tool used during Leg 203 is a neutron-neutron device. Its detectors record both the numbers of neutrons arriving at various distances from the source and neutron ar-

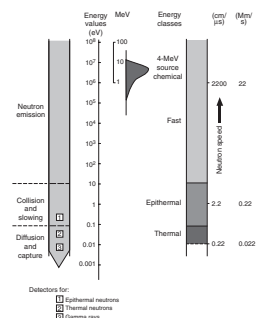
F10. Compton scattering of gamma rays, p. 41.



F11. Schematic drawing of compensated neutron tool, p. 42.



F12. Schematic diagram of a neutron life, p. 43.



rival times, which act as a measure of formation porosity. However, as hydrogen bound in minerals such as clays or in hydrocarbons also contributes to the measurement, the raw porosity value is often an overestimate.

### Electrical Resistivity

Two types of resistivity measurement tools are available on board: the Dual Laterolog (DLL) and the DIT. The former has a response range of 0.2–40,000  $\Omega\text{m}$  and measures the direct resistivity of a formation. It is mostly applied in medium- to high-resistivity formations in igneous environments (e.g., oceanic basalts and gabbros). The DIT, with a response range of 0.2–2,000  $\Omega\text{m}$ , is a conductivity-sensitive device and is most commonly applied in low- to medium-resistivity formations such as sediments. However, it has also produced very good results in ocean-crust basalts.

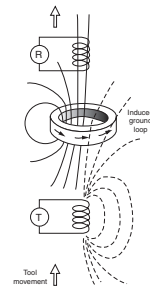
The DIT has a deep induction phasor-processed device (IDPH), a medium induction phasor-processed device (IMPH), a spherically focused resistivity measurement (SFLU), and a spontaneous potential (SP) device. The two induction devices transmit high-frequency alternating currents through transmitter coils, creating time-varying magnetic fields that induce currents in the formation (Fig. F13). These induced currents create, in turn, a magnetic field that induces new currents in the receiver coils, producing a voltage. The currents are proportional to the conductivity of the formation, as is the voltage. The SFLU is a shallow-penetration galvanic device that measures the current necessary to maintain a constant voltage drop across a fixed interval of the formation. In high-resistivity formations (>100  $\Omega\text{m}$ ), both IDPH and IMPH measurements may be erroneous, but the error can be greatly reduced by downhole calibration. In such cases, SFLU measurements produce good results, similar to the DLL device (Shipboard Scientific Party, 1998). The resistivity of a rock is controlled largely by the porosity of the rock, the properties of the pore fluid(s), and the connectivity of the pores.

Spontaneous potentials can originate from a variety of causes, electrochemical, electrothermal, and electrokinetic streaming potentials, and membrane potentials as a result of differences in the mobility of ions in the pore and drilling fluids. SP may be useful to infer fluid-flow zones and formation permeability (Fig. F14).

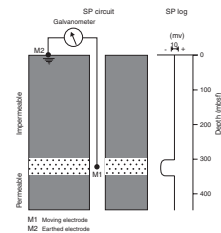
### Temperature, Acceleration, and Pressure

Downhole temperature, acceleration, and pressure were measured with the LDEO high-resolution TAP. When attached to the bottom of the triple combo string, the TAP operates in an autonomous mode with data stored in built-in memory. A two-component thermistor, for different temperature ranges, is mounted near the bottom of the tool in the slotted protective cover. The time constant of the thermistor assembly in water is ~0.4 s. The tool includes a pressure transducer (0–10,000 psi), which is used to activate the tool at a specified depth and perform pressure measurements. The TAP also incorporates a high-sensitivity vertical accelerometer, providing data for analyzing the effects of heave on a deployed tool string, and an internal temperature sensor for monitoring the temperature inside the electronic cartridge. Temperature and pressure data are recorded once per second, and accelerometer data can be recorded at a 4- or 8-Hz sampling rate.

F13. The principle of the simple induction tool, p. 44.



F14. Principle of the SP log, p. 45.



The borehole temperature record provides information on the thermal regime of the surrounding formation. The vertical heat flow can be estimated from the vertical temperature gradient combined with measurements of the thermal conductivity from core samples. The temperature record must be interpreted with caution, as the amount of time elapsed between the end of drilling and the logging operation is generally not sufficient to allow the borehole to recover thermally from the influence of drilling fluid circulation. The data recorded under such circumstances may differ significantly from thermal equilibrium for that environment. Nevertheless, from the spatial temperature gradient it is possible to identify abrupt temperature changes that may represent localized fluid flow into the borehole indicative of fluid pathways and fracturing and/or breaks in the temperature gradient that may correspond to contrasts in permeability at lithologic boundaries.

### Acoustic Measurements

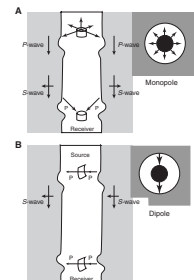
Sonic velocities were measured with the DSI. The DSI tool employs a combination of monopole and dipole transducers (Fig. F15) to make accurate measurements of sonic wave velocities in a wide variety of lithologies (Schlumberger, 1995). The tool measures the transit times between sonic transmitters and an array of eight receivers. It averages replicate measurements, providing a direct measurement of sound velocity through the formation that is relatively free from environmental effects, such as formation damage and enlarged borehole (Schlumberger, 1989). Along with the monopole transmitters found on most sonic tools, the DSI has two crossed dipole transmitters. Thus, the DSI can be used to determine  $S$ -wave velocity in all types of formations. When the formation shear velocity is less than the borehole fluid velocity, particularly in unconsolidated sediments, the flexural wave travels at the  $S$ -wave velocity and is the most reliable way to estimate a shear velocity log. The omnidirectional source generates  $P$ -,  $S$ -, and Stoneley waves in hard formations at the borehole/formation interface. The configuration of the DSI also allows recording of cross-line dipole waveforms, which can be used to estimate  $S$ -wave splitting caused by preferred mineral and/or structural orientations in consolidated formations. A low-frequency source (80 Hz) enables Stoneley waveforms to be acquired as well. These “guided” waves are associated with the solid/fluid boundary at the borehole wall, and their amplitude decays exponentially away from the boundary in both the fluid and the formation.

In addition, information such as  $P$ -,  $S$ -, and Stoneley wave amplitudes,  $S$ -wave polarization, and Poisson’s ratio can be extracted post-cruise to provide information about lithology, porosity, and anisotropy. Amplitude processing and stacking of Stoneley wave reflections can also be used to identify fractures, fracture permeability, and aperture in the vicinity of the borehole. The tool configuration and data processing procedures are described in detail in the Leg 174B *Initial Reports* volume (Becker, Malone, et al., 1998).

### Accelerometry and Magnetic Field Measurement

Downhole magnetic field and acceleration measurements were performed with the GPIT. The GPIT is usually used in combination with the FMS, but it can be attached to other tools or run autonomously. The primary purpose of this sonde, which incorporates a three-component accelerometer and a three-component magnetometer, is to determine

F15. Array sonic transmitter types, p. 46.

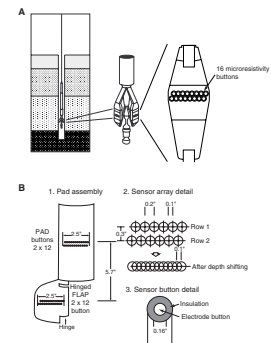


the acceleration and orientation of the FMS-sonic tool string during logging. The acceleration data allow more precise determination of log depths than is possible based on cable length alone, as the wireline is subject to both stretching and ship heave. Acceleration data are also used in processing of FMS data to correct the images for irregular tool motion. A third application of the acceleration data is the measurement of the hole deviation (in degrees). The magnetic measurements of inclination may be affected by the magnetization of the casing and/or drill pipe. Furthermore, local magnetic anomalies, generated by high remnant magnetization of basalts in the basement section of a borehole, can interfere with the determination of tool orientation. However, these magnetic measurements can be useful for constraining the magnetic stratigraphy of the basement section.

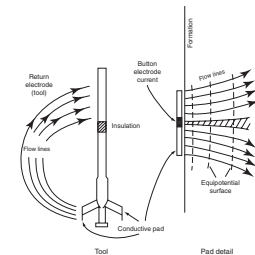
### Electrical Images

The FMS provides high-resolution electrical resistivity based images of borehole walls. The tool has four orthogonal arms (pads), each containing 16 microelectrodes, or “buttons,” which are pressed against the borehole wall during recording. The electrodes are arranged in two diagonally offset rows of eight electrodes each and are spaced ~2.5 mm apart (Fig. F16). A focused current is emitted from each button of the four pads into the formation with a return electrode near the top of the tool (Fig. F17). Array buttons on each of the pads measure current intensity variations. The FMS image is sensitive to structures within ~25 cm of the borehole wall and has a vertical resolution of 5 mm with a coverage of 25% of the borehole wall for a borehole diameter of 9 7/8 in (25.1 cm) (i.e., RCB bit size). FMS logging commonly includes two passes, which merge the images together to improve borehole wall coverage. To produce reliable FMS images, however, the pads must be pressed firmly against the borehole wall. The maximum extension of the caliper arms is 15.0 in (38.1 cm). In holes with a diameter >15 in (38.1 cm), the pad contact will be inconsistent and the FMS images can be blurred. The maximum borehole deviation where good data can be obtained with this tool is 10°. Irregular borehole walls also adversely affect the images as contact with the wall is poor. FMS images are oriented to local magnetic north using the GPIT (see “**Accelerometry and Magnetic Field Measurement,**” p. 23). Processing transforms these measurements of microresistivity variations into continuous, spatially oriented, and high-resolution images that display geologic structures behind the borehole walls. Further processing can provide measurements of dip and direction (azimuth) of planar features in the formation. This allows the dip and azimuth of geological features intersecting the hole to be measured from processed FMS images. FMS images are particularly useful for mapping structural features, dip, detailed core-log correlation, and positioning of core sections where there is poor recovery. The FMS images can be used to compare logs visually with core to ascertain the orientations of bedding, fracture patterns, and sedimentary structures. FMS images have proved particularly valuable in the interpretation of sedimentary, as well as igneous structures, in previous ODP legs and determination of volcanic sequences (Ayadi et al., 1998, Brewer et al., 1999). Detailed interpretations of FMS images in combination with other log data and core imaging will be conducted postcruise.

F16. Schematic diagram of FMS and FMI, p. 47.



F17. Electrical flow characteristics of the FMI, p. 48.





## Seismic Measurements

The WST is a single-axis check-shot tool used for zero-offset VSPs. The tool consists of a single geophone, pressed against the borehole wall, with a sampling interval of 1 ms. It is used to record the acoustic waves generated by a seismic source located near the sea surface. A GI gun (Sodera 210-in<sup>3</sup> Harmonic) was used as a seismic source (Fig. F8). The gun, which produces waves with a frequency content exceeding 200 Hz, was suspended by a buoy at a depth of 2–3 meters below sea level, offset 55.8 m from the hole on the portside of the ship. Two hydrophones (one Schlumberger and one ODP hydrophone) were used (Fig. F8) to record the break signal. The Schlumberger hydrophone was suspended 2 m below the gun, and the other hydrophone was attached directly to the GI gun. Several test shots (~30–40 shots) were fired while the tool was lowered down to the bottom of the hole (BOH) and on the BOH itself. During these tests, it turned out that the first break of the lower hydrophone was poor. Instead, data obtained from the upper hydrophone gave a very good break signal, although the data were of limited use for source behavior because of the proximity of the hydrophone to the surface.

During operations in Hole 1243B, the WST was clamped against the borehole wall at intervals of 10 m, and the gun fired 10 times at intervals of 20 s. The resulting waveforms were stacked. A traveltime was determined from the first break in each trace. In general, the acoustic velocities determined from the sonic tool differ significantly from the seismic velocities because of frequency dispersion (e.g., the DSI operates at 10–20 kHz vs. 50–100 Hz in seismic data) and because the sound is forced to travel along the borehole wall, a path that is quite different from the one taken by the gun signal generated during a seismic reflection survey. One of the applications of data from the WST is a plot of depth vs. traveltime determined from check shots. This plot is used to calibrate the sonic logs and determine accurate drilling depths and their relative position with respect to targets on seismic reflection profiles. The seismic reflection survey conducted at the beginning of Leg 203, however, used a small water gun source and did not provide useful data within the basement. Thus, direct comparisons of WST measurements and these seismic data are not possible.

## Log Data Quality

The quality of log data can be seriously degraded by excessively wide sections of the borehole or by rapid changes in the hole diameter. If the borehole is irregular, wide, or there are many washouts, there may be problems with those tools that require good contact with the wall (density, porosity, and FMS). Resistivity and velocity measurements are the least sensitive to borehole effects. Nuclear measurements (density, neutron porosity, and both natural and induced spectral gamma rays) are mainly affected by borehole fluid and/or drilling mud signal attenuation. Corrections can be applied to the original data to reduce the effects of these conditions and, generally, any departure from the conditions under which the tool was calibrated.

The depth of the wireline logging measurements is determined from the length of the logging cable paid out at the winch on the ship. Small errors in depth matching can distort the logging results in zones of rapidly changing lithology. Logs from different tool strings may have depth mismatches caused by either cable stretch or ship heave during

recording. To minimize the effects of ship heave, a hydraulic WHC adjusts for rig motion during logging operations. Distinctive features recorded by the NGT, run on the FMS-sonic tool string (Hole 1243B) and on the CBT (Hole 1243A), provide calibration points and relative depth offsets among the logging runs and can be correlated with distinctive lithologic contacts observed in the core recovery or drilling penetration (e.g., pillow basalt–breccia transitions). The coring depth (drillers depth) is determined from the known length of the BHA and pipe stands. Discrepancies between the drillers depth and the wireline log depth occur because of core expansion, incomplete core recovery, drill pipe stretch in the case of drill pipe depth, cable stretch (~1 m/km), as well as cable slip in the case of log depth. Tidal changes in sea level, up to 1 m in the open ocean, will also have an effect. Precise core-log depth matching is difficult in zones where core recovery is low because of the inherent ambiguity of placing the recovered section within the cored interval.

### **Data Recording and Processing**

Data for each logging run are recorded, stored digitally, and monitored in real time using the MCM. Measurements are performed and recorded on downhole and uphole logging runs. Whereas the downward measurements are taken for reference, tools are only partly operational because calipers have to be closed going downward, the upward runs are the actual logging runs. The tool string is pulled up at constant speed to provide continuous measurements as a function of depth of several properties simultaneously. The TAP is deployed as an autonomous recording tool. The preparation and data processing of the TAP are done in the Downhole Measurements Laboratory (DHML) using a specialized acquisition system. On completion of logging, data from the Schlumberger tools are transferred to the DHML for preliminary interpretation. Basic processing is then carried out to provide scientists with a comprehensive quality-controlled downhole log data set that can be used for comparison and integration with other data collected during Leg 203. Extended processing is usually carried out onshore at LDEO after the data are transmitted by satellite from the ship. These analyses include adjustments to remove depth offsets between data from different logging runs, corrections specific to certain tools and logs, documentation for the logs (with an assessment of log quality) and conversion of the data to a widely accessible format (ASCII for the conventional logs and GIF for the FMS images). Schlumberger GeoQuest's software package, GeoFrame, is used for most of the processing. Further postcruise processing of FMS log data is performed, and data are available 1 month after the cruise.

Processed acoustic, caliper, density, gamma ray, magnetic, neutron porosity, resistivity, and temperature data in ASCII format are available directly from the LDEO-BRG Internet site at: [www.ldeo.columbia.edu/BRG/ODP/DATABASE](http://www.ldeo.columbia.edu/BRG/ODP/DATABASE). A summary of logging highlights is also posted on the LDEO-BRG Web site at the end of each leg.

### **UNDERWAY GEOPHYSICS**

While transiting from Panama to Site 1243 and from Site 1243 to Victoria, we carried out 3.5-kHz echo sounding and magnetometer surveys. In addition, as we approached Site 1243, we collected a series of

single-channel seismic reflection lines to define a precise location for drilling. The survey was quite successful, and the data were used primarily to measure sediment thickness and water depth.

A site survey for Leg 138 had also been conducted during the previous century (Mayer et al., 1992), but the density of seismic and bathymetric lines was inadequate to place a long-term observatory with respect to the bottom topography.

## Navigation

Navigation data were acquired throughout the leg on an Ashtech GG24 Global Positioning System (GPS) receiver. The antenna was mounted on the starboard stack 46.33 m aft of the moonpool (Fig. F18), although the datum is the moonpool itself. GPS fixes were recorded by WINFROG navigation software every 60 s, except during water gun shooting, when they were recorded at each shot instant (9 s). Generic Mapping Tools (GMT) software (Wessel and Smith, 1995) was used to process and display the navigation data on SUN workstations.

## Time

The time datum for all underway geophysics activities is Universal Time Coordinated (UTC) as provided from the Ashtech receiver. If communication between the Ashtech receiver and the satellite is interrupted, the receiver uses its own internal clock to maintain the time base. The WINFROG navigation system displays the UTC time many times per second, but the internal clocks of the data acquisition systems are not accurately or continuously synchronized to UTC. During this cruise, we used the WINFROG navigation system to send a trigger pulse to the water gun based on WINFROG's internal clock. The time stamp on the seismic data comes from the SUN workstation internal clock, which was synchronized manually with UTC. The underway geophysics data were acquired using the A2D package (University of Hawaii software running on a SUN workstation). A2D has the time referenced approximately to UTC, whereas the trigger pulses from WINFROG are based on the WINFROG clock, which may not be precisely synchronized to UTC. We did note that A2D might have dropped a few shots during the survey because of a differential shot count between WINFROG triggers (larger count) and A2D records (smaller count). The greatest possible cumulative error in timing, as a result of the discrepancy in counts, is ~90 s over the 6-hr survey period. At a survey speed of 5 kt, this is equivalent to a 225-m uncertainty over ~22 km of track line, or 1%.

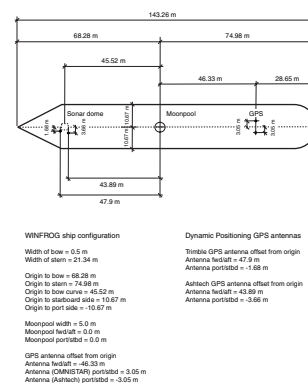
## Magnetics

The magnetic data were acquired with an EG&G Geometrics Marine proton precession Magnetometer (model G-886) towed 500 m astern. Values of total field intensity were acquired every 60 s using the WINFROG navigation software on a PC with a Microsoft windows operating system.

## Bathymetry

The underway 3.5-kHz echo sounder data were acquired using an EDO model 515A-250 transducer mounted in a sonar dome located

F18. Dimensions to correct GPS location to the moonpool, p. 49.



45.52 m forward of the moonpool. The 3.5-kHz transceiver is a Raytheon model PTR-105 with a maximum 2-kW output. The data were processed in real time using a Raytheon Correlator echo sounder processor (CESP III). Uncorrected depths were recorded on an EPC 8082 analog line-scan recorder. These were read visually from the recorders every 5 min and were entered into a Microsoft Excel spreadsheet by the underway technician. The line-scan recorder was automatically annotated with ship's speed and heading every 5 min and ship's position every 30 min. These annotations were also logged by WINFROG. Uncorrected depths convert traveltime to nominal depth assuming a sound velocity in seawater of 1500 m/s. Corrected depths (using Matthews' Tables to allow for the varying sound speed with depth and location in the ocean [Carter, 1980]) were computed by hand for each site.

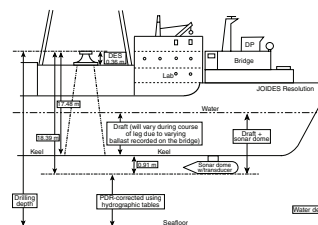
The transducer element is 0.91 m below the keel of the ship and 18.39 m below the dual elevator system (the reference datum for drilling activities). Water depth relative to sea level was obtained by adding 0.91 m and the mean draft (typically,  $6.5 \pm 0.6$  m) to the corrected echo sounder depth. Figure F19 is a schematic of the ship, which summarizes some of the key dimensions used in computing depth to various locations.

### Seismic System

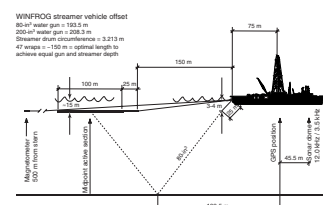
The acoustic source consisted of a single 80-in<sup>3</sup> water gun developed by Seismic Systems Inc. (SSI) (Hutchinson and Detrick, 1984). In general, the SSI water gun was fired at a rate faster than is typical in order to maximize horizontal resolution. A 60-phone 100-m-long Teledyne oil-filled streamer recorded the water gun shots. The streamer was towed ~15 m deep, ~225 m astern (Fig. F20). The midpoint between the water gun and the active streamer's midpoint was 188 m astern the ship's recorded GPS position. Streamer output was split to enable it to be used for real-time analog displays on EPC facsimile recorders and for digitizing and recording of SEG-Y files on 4-mm DAT tape and 8-mm EXABYTE tape using SUN workstations. Digital data were subsequently processed using SIOSEIS software (Henkart, 1992).

We conducted a test of the seismic system on 7 June, with the result that one water gun was found to be inoperable, one gun failed in the water, and the streamer was insensitive. Following repairs, the tests were repeated on 8 June with excellent results. The survey itself (10 June) was conducted with outstanding results, although one water gun failed during the survey and had to be replaced.

**F19.** Significant depth dimensions on the ship, p. 50.



**F20.** Depths and ranges for the single-channel seismic acquisition and magnetometer systems, p. 51.



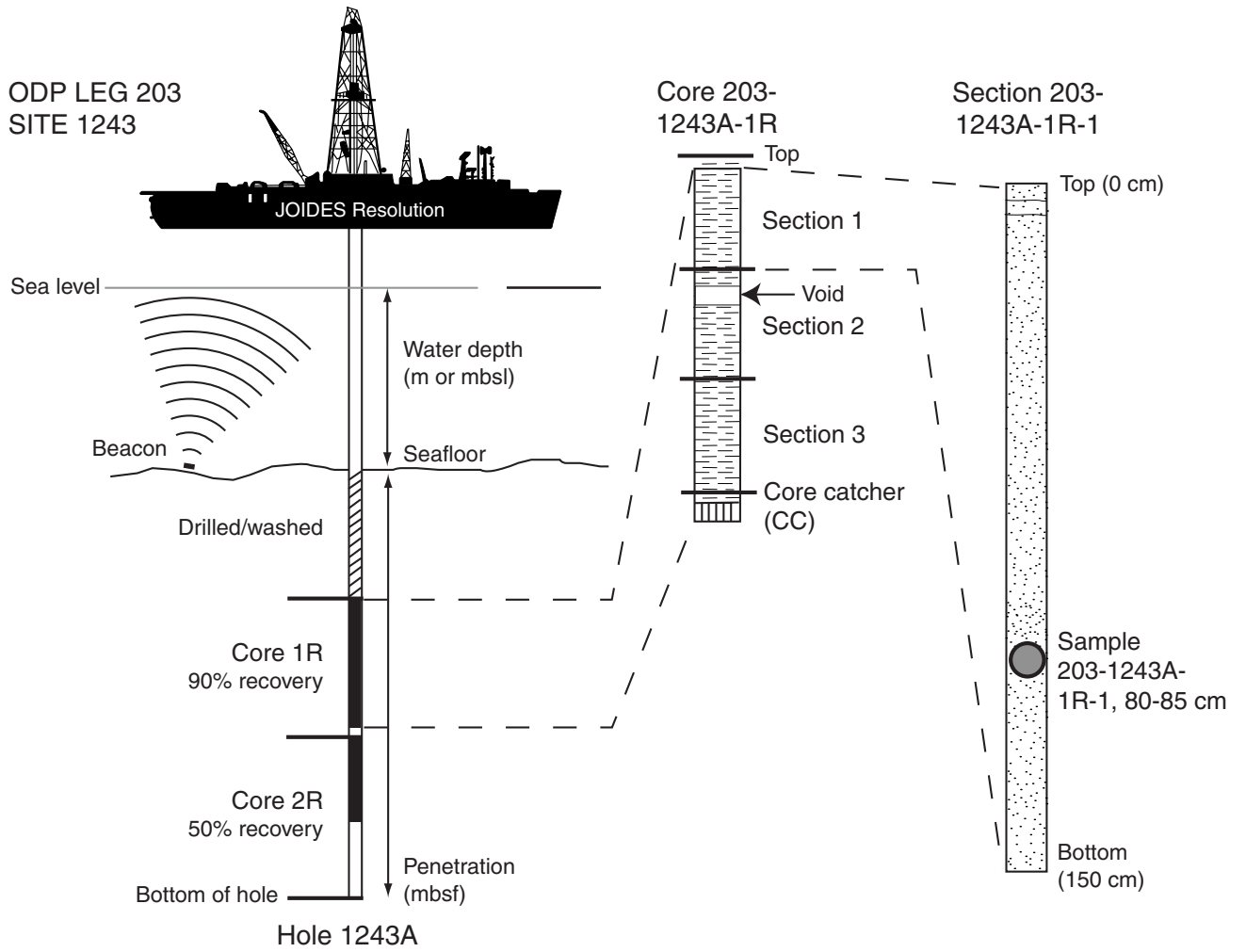
## REFERENCES

- ASTM, 1989. *Annual Book of ASTM Standards (Part 19): Natural Building Stones: Soil and Rock*: Philadelphia (Am. Soc. Testing and Mater.).
- Ayadi, M., Pezard, P.A., Laverne, C., and Bronner, G., 1998. Multi-scalar structure at DSDP/ODP Site 504, Costa Rica Rift, I: stratigraphy of eruptive products and accretion processes. In Harvey, P.K., and Lovell, M.A. (Eds.), *Core-Log Integration*. Spec. Publ.—Geol. Soc. London, 136:297–310.
- Balsam, W.L., and Damuth, J.E., 2000. Further investigations of shipboard vs. shore-based spectral data: implications for interpreting Leg 164 sediment composition. In Paull, C.K., Matsumoto, R., Wallace, P., and Dillon, W.P. (Eds.), *Proc. ODP, Sci. Results*, 164: College Station, TX (Ocean Drilling Program), 313–324.
- Balsam, W.L., Damuth, J.E., and Schneider, R.R., 1997. Comparison of shipboard vs. shore-based spectral data from Amazon-Fan cores: implications for interpreting sediment composition. In Flood, R.D., Piper, D.J.W., Klaus, A., and Peterson, L.C. (Eds.), *Proc. ODP, Sci. Results*, 155, 193–215 [CD-ROM]. Available from: Ocean Drilling Program, Texas A&M University, College Station, TX 77845-9547, U.S.A.
- Balsam, W.L., Deaton, B.C., and Damuth, J.E., 1998. The effects of water content on diffuse reflectance measurements of deep-sea core samples: an example from ODP Leg 164 sediments. *Mar. Geol.*, 149:177–189.
- Becker, K., Malone, M.J., et al., 1998. *Proc. ODP, Init. Repts.*, 174B: College Station, TX (Ocean Drilling Program).
- Blum, P., 1997. Physical properties handbook: a guide to the shipboard measurement of physical properties of deep-sea cores. *ODP Tech. Note*, 26 [Online]. Available from World Wide Web: <<http://www-odp.tamu.edu/publications/tnotes/tn26/INDEX.HTM>>. [Cited 2002-05-29]
- Boggs, S., 1995. *Principles of Sedimentology and Stratigraphy* (2nd ed.): Upper Saddle River, NJ (Prentice-Hall, Inc.).
- Borehole Research Group, 1990. *Ocean Drilling Program Logging Manual*, LDEO.
- Boyce, R.E., 1976. Definitions and laboratory techniques of compressional sound velocity parameters and wet-water content, wet-bulk density, and porosity parameters by gravimetric and gamma-ray attenuation techniques. In Schlanger, S.O., Jackson, E.D., et al., *Init. Repts. DSDP*, 33: Washington (U.S. Govt. Printing Office), 931–958.
- Brewer, T.S., Harvey, P.K., Lovell, M.A., Haggas, S., Pezard, P.A., and Goldberg, D., 1999. Borehole images of the ocean crust: case histories from the Ocean Drilling Program. In Lovell, M.A., Williamson, and Harvey, P.K. (Eds.), *Borehole Images: Application and Case Histories*. Spec. Publ.—Geol. Soc. London, 159:283–294.
- Carter, D.J.T., 1980. *Echo-Sounding Correction Tables (Formerly Matthews' Tables)*: Taunton, Somerset, UK (Hydrographic Dept., Min. of Defence).
- Desbrandes, R., 1985. *Encyclopedia of Well Logging*. Institut Francais Du Pétrole Publications, Éditions Technip.
- Dunham, R.J., 1962. Classification of carbonate rocks according to depositional texture. In Ham, W.E. (Ed.), *Classification of Carbonate Rocks*. AAPG Mem., 108–121.
- Ekstrom, M.P., Dahan, C., Chen, M.-Y., Lloyd, P., and Rossi, D.J., 1987. Formation imaging with microelectrical scanning arrays. *Log Analyst*, 28:294–306.
- Ellis, D.V., 1987. *Well Logging for Earth Scientists*: New York (Elsevier).
- Folk, R.L., 1962. Spectral subdivision of limestone types. In Ham, W.E. (Ed.), *Classification of Carbonate Rocks*. AAPG Mem., 1:-62–68.
- Goldberg, D., 1990. Test performance of the Ocean Drilling Program wireline heave motion compensator. *Sci. Drill.*, 1:206–209.
- , 1997. The role of downhole measurements in marine geology and geophysics. *Rev. Geophys.*, 35:315–342.
- Henkart, P., 1992. SIOSEIS—a computer system for enhancing and manipulating marine seismic reflection and refraction data. *Tech. Rpt., Scripps Inst. of Oceanogr.*

- Hutchinson, D.R., and Detrick, R.S., 1984. Water gun vs. air gun: a comparison. *Mar. Geophys. Res.*, 6:295–310.
- Kirschvink, J.L., 1980. The least-squares line and plane and the analysis of palaeomagnetic data. *Geophys. J. R. Astron. Soc.*, 62:699–718.
- Lavenda, B.H., 1985. Brownian motion. *Sci. Am.*, 252:56–67.
- Lovell, M.A., Harvey, P.K., Brewer, T.S., Williams, C., Jackson, P.D., and Williamson, G., 1998. Application of FMS images in the Ocean Drilling Program: an overview. In Cramp, A., MacLeod, C.J., Lee, S.V., and Jones, E.J.W. (Eds.), *Geological Evolution of Ocean Basins: Results from the Ocean Drilling Program*. Spec. Publ.—Geol. Soc. London, 131:287–303.
- MacKenzie, W.S., Donaldson, C.H., and Guilford, C., 1982. *Atlas of Igneous Rocks and their Textures*: Harlow, England (Longman).
- Mayer, L., Piasias, N., Janecek, T., et al., 1992. *Proc. ODP, Init. Repts.*, 138 (Pts. 1 and 2): College Station, TX (Ocean Drilling Program).
- Mayer, L.A., Piasias, N.G., Mix, A.C., Lyle, M.W., Arason, P., and Mosher, D., 1992. Site surveys. In Mayer, L., Piasias, N., Janecek, T., et al., *Proc. ODP, Init. Repts.*, 138 (Pt. 1): College Station, TX (Ocean Drilling Program), 93–100.
- Mazzullo, J.M., Meyer, A., and Kidd, R.B., 1988. New sediment classification scheme for the Ocean Drilling Program. In Mazzullo, J., and Graham, A.G. (Eds.), *Handbook for Shipboard Sedimentologists*. *ODP Tech. Note*, 8:45–67.
- Munsell Color Company, Inc., 1994. *Munsell Soil Color Chart* (Revised ed.): Newburgh, MD (Munsell Color).
- Murray, R.W., Miller, D.J., and Kryc, K.A., 2000. Analysis of major and trace elements in rocks, sediments, and interstitial waters by inductively coupled plasma–atomic emission spectrometry (ICP–AES). *ODP Tech. Note*, 29 [Online]. Available from World Wide Web: <<http://www-odp.tamu.edu/publications/tnotes/tn29/INDEX.HTM>>. [Cited 2002-05-29]
- Owen, J.D., 1966. A review of fundamental nuclear physics applied to gamma ray spectral logging. *Log Analyst*, Sept–Oct, 37–47.
- Rider, M.H., 1996. *The Geological Interpretation of Well Logs* (2nd ed.): Caithness (Whittles Publishing).
- Rock-Color Chart Committee, 1991. *Rock Color Charts*. Geol. Soc. Am.
- Rothwell, R.G., 1989. *Minerals and Mineraloids in Marine Sediments: An Optical Identification Guide*: Basking, UK (Elsevier Appl. Sci. Publ.).
- Schlumberger, 1989. *Log Interpretation Principles/Applications*: Houston (Schlumberger Educ. Services), SMP-7017.
- , 1994a. *IPL Integrated Porosity Lithology*: Houston (Schlumberger Wireline and Testing), SMP-9270.
- , 1994b. *FMI Fullbore Formation MicroImager*: Houston (Schlumberger Educational Services).
- , 1995. *DSI—Dipole Sonic Imager*: Houston (Schlumberger Wireline and Testing), SMP-5128.
- Seismic Systems Manual, 2000. *Operation and Maintenance Manual: G.I Gun*: Houston (Seismic Systems, Inc).
- Serra, O., 1979. Diagraphies différées; bases de l'interprétation, Tome 1. Acquisition des données diagraphiques. *Bull. Cent. Rech. Explor.-Prod. Elf Aquitaine*, Mem. 1.
- , 1986. *Fundamentals of Well-Log Interpretation* (Vol. 2): *The Interpretation of Logging Data*. Dev. Pet. Sci., 15B.
- , 1984. *Fundamentals of Well-Log Interpretation* (Vol. 1): *The Acquisition of Logging Data*: Dev. Pet. Sci., 15A.
- , 1989. *Formation MicroScanner Image Interpretation*: Houston (Schlumberger Educ. Services), SMP-7028.
- Shipboard Scientific Party, 2003. Explanatory notes. In Stephen, R.S., Kasahara, J., Acton, G.D., et al., *Proc. ODP, Init. Repts.*, 200 [CD-ROM]. Available from: Ocean Drilling Program, Texas A&M University, College Station TX 77845-9547, USA.


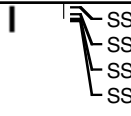
- , 1997. Explanatory notes. *In* Eberli, G.P., Swart, P.K., Malone, M.J., et al., *Proc. ODP, Init. Repts.*, 166: College Station, TX (Ocean Drilling Program), 43–65.
- , 1998. Introduction. *In* Becker, K., Malone, M.J., et al., *Proc. ODP, Init. Repts.*, 174B: College Station, TX (Ocean Drilling Program), 3–9.
- , 2002. Explanatory notes. *In* Tarduno, J.A., Duncan, R.A., Scholl, D.W., et al., *Proc. ODP, Init. Repts.*, 197 [CD-ROM]. Available from: Ocean Drilling Program, Texas A&M University, College Station TX 77845-9547, USA.
- Terry, R.D., and Chilingar, G.V., 1955. Summary of “Concerning some additional aids in studying sedimentary formations” by M.S. Shvetsov. *J. Sediment. Petrol.*, 25:229–234.
- Tittle, C.W., 1961. Theory of neutron logging. *Geophysics*, 26:27–39.
- Vacquier, V., 1985. The measurement of thermal conductivity of solids with a transient linear heat source on the plane surface of a poorly conducting body. *Earth Planet. Sci. Lett.*, 74:275–279.
- von Herzen, R.P., and Maxwell, A.E., 1959. The measurement of thermal conductivity of deep-sea sediments by a needle-probe method. *J. Geophys. Res.*, 64:1557–1563.
- Wessel, P., and Smith, W.H.F., 1995. New version of the Generic Mapping Tools released. *Eos, Trans. Am. Geophys. Union*, 76:329.
- Zemanek, J., Williams, D.M., and Schmidt, D.P., 1991. Shear-wave logging using multipole sources. *Log Analyst*, 32:233–241.
- Zijderveld, J.D.A., 1967. A. C. demagnetization of rocks: analysis of results. *In* Collinson, D.W., Creer, K.N., and Runcorn, S.K. (Eds.), *Methods in Paleomagnetism*: Amsterdam (Elsevier), 254–286.

Figure F1. Schematic diagram illustrating hole, core, section, and sample numbering.





**Figure F2.** An example of an AppleCORE barrel sheet. GRAPHIC LITH. = graphic lithology, ICHNO. = ich-nofossils, DISTURB. = disturbance.

Site 1243 Hole B Core 1R Cored 102.0-108.6 mbsf										
METERS	CORE AND SECTION	GRAPHIC LITH.	BIOTURB.	STRUCTURE	ACCESSORIES	ICHNO.	FOSSILS	DISTURB.	SAMPLE	DESCRIPTION
										 <p>Core consists of firm nannofossil ooze pieces in a matrix of more disturbed mud. The core arrived on deck as lumps of sediment in muddy water. The "core" represents the arrangement when the assemblage was compressed into the end of the liner. Lumps and their matrix are orange and brown in color.</p>

**Figure F3.** An example of a Leg 203 electronic hard rock visual core description.

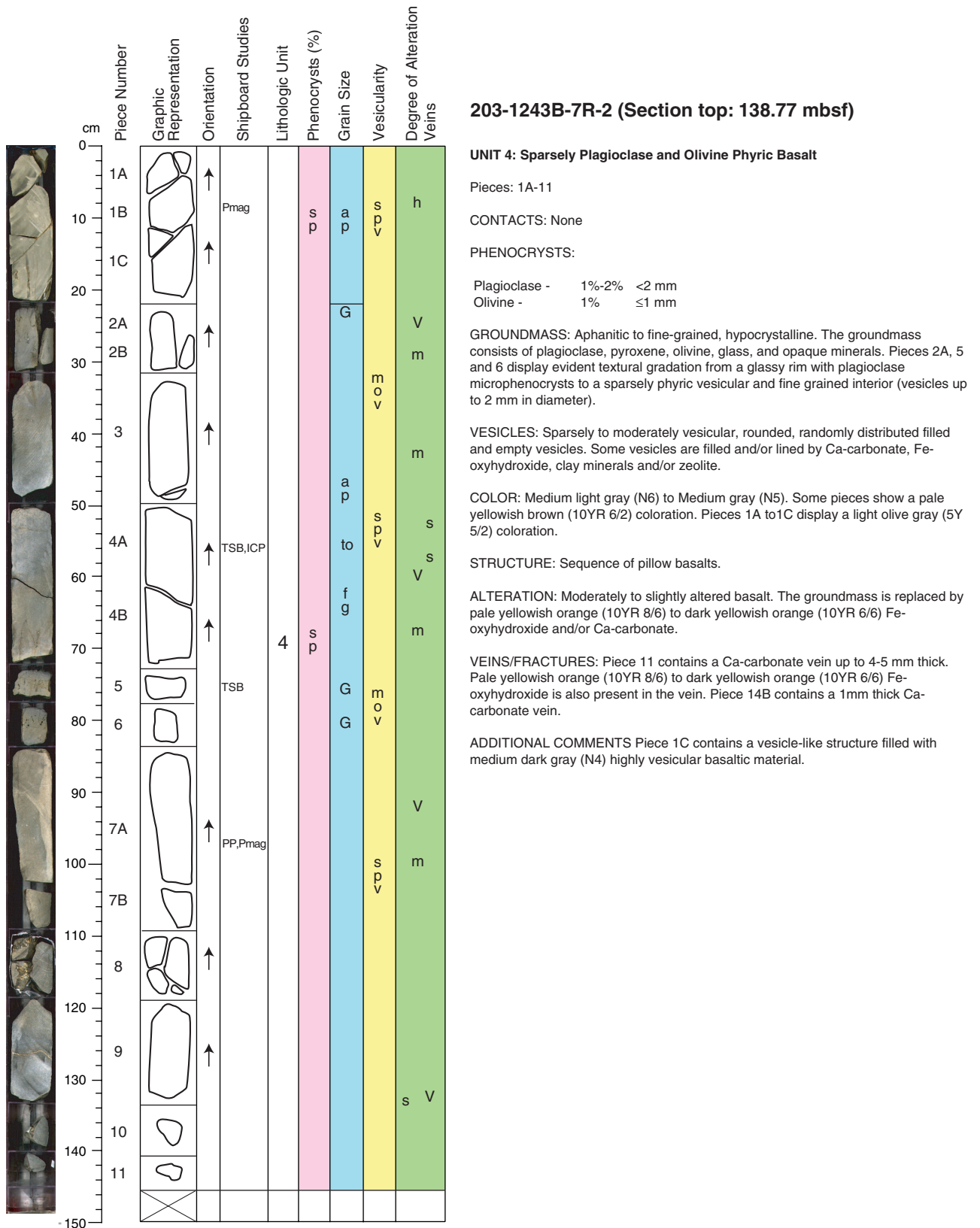
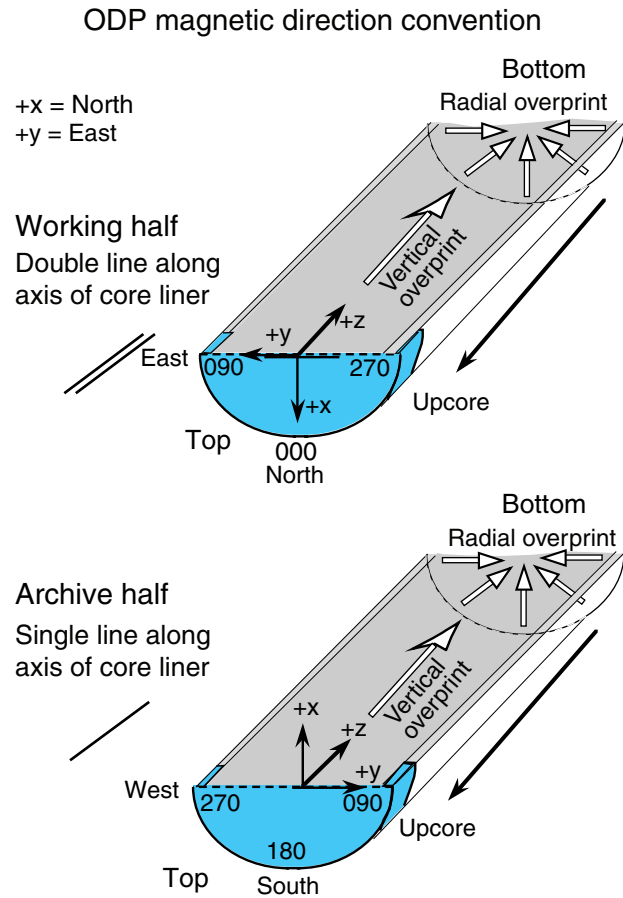


Figure F4. Key to the electronic hard rock visual core description.

**Igneous texture/structures definitions and abbreviations**

Phenocryst		a Aphyric (<1%)	s p Sparsely phyric (1%-2%)	m p Moderately phyric (2%-10%)	h p Highly phyric (>10%)		
Grain size		G Glass	a p Aphanitic (<1 mm)	f g Fine grained (1-2 mm)	m g Medium grained (2-5 mm)		
Vesicularity		n v Nonvesicular (<1%)	s p v Sparsely vesicular (1%-5%)	m o v Moderately vesicular (5%-20%)	h i v Highly vesicular (>20%)		
Degree of alteration		f Unaltered (<2%)	s Slight (2%-10%)	m Moderate (10%-40%)	h High (40%-80%)	vh Very high (80%-95%)	c Complete (95%-100%)
Veins		V Veins present					

Figure F5. ODP paleomagnetic coordinate system for archive and working halves with radial and vertical overprints shown (Shipboard Scientific Party, 2003). The radially inward overprint has been observed during many previous cruises (e.g., Shipboard Scientific Party, 1997).



**Figure F6.** The triple combo, FMS-sonic, and the WST tool strings.

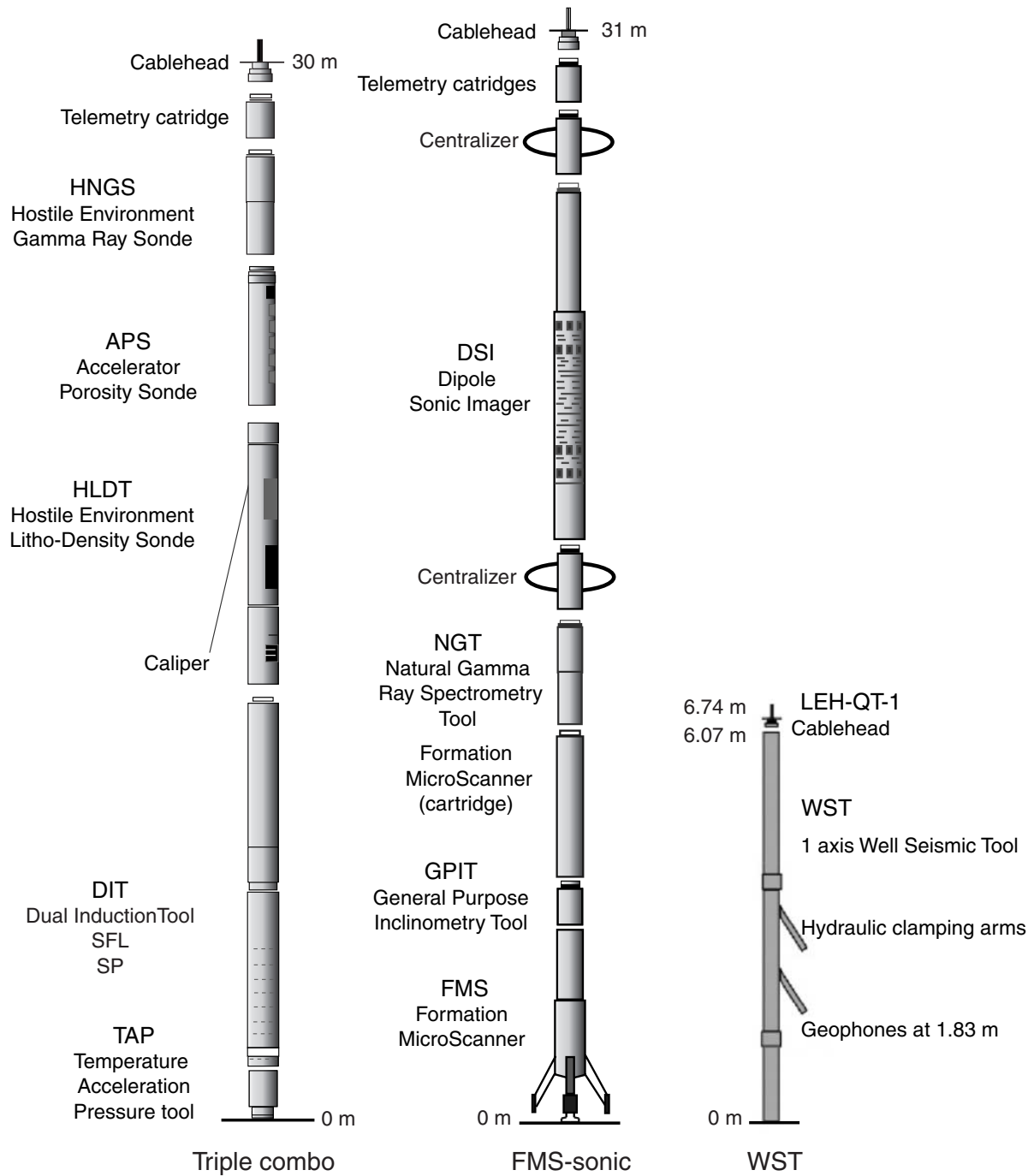
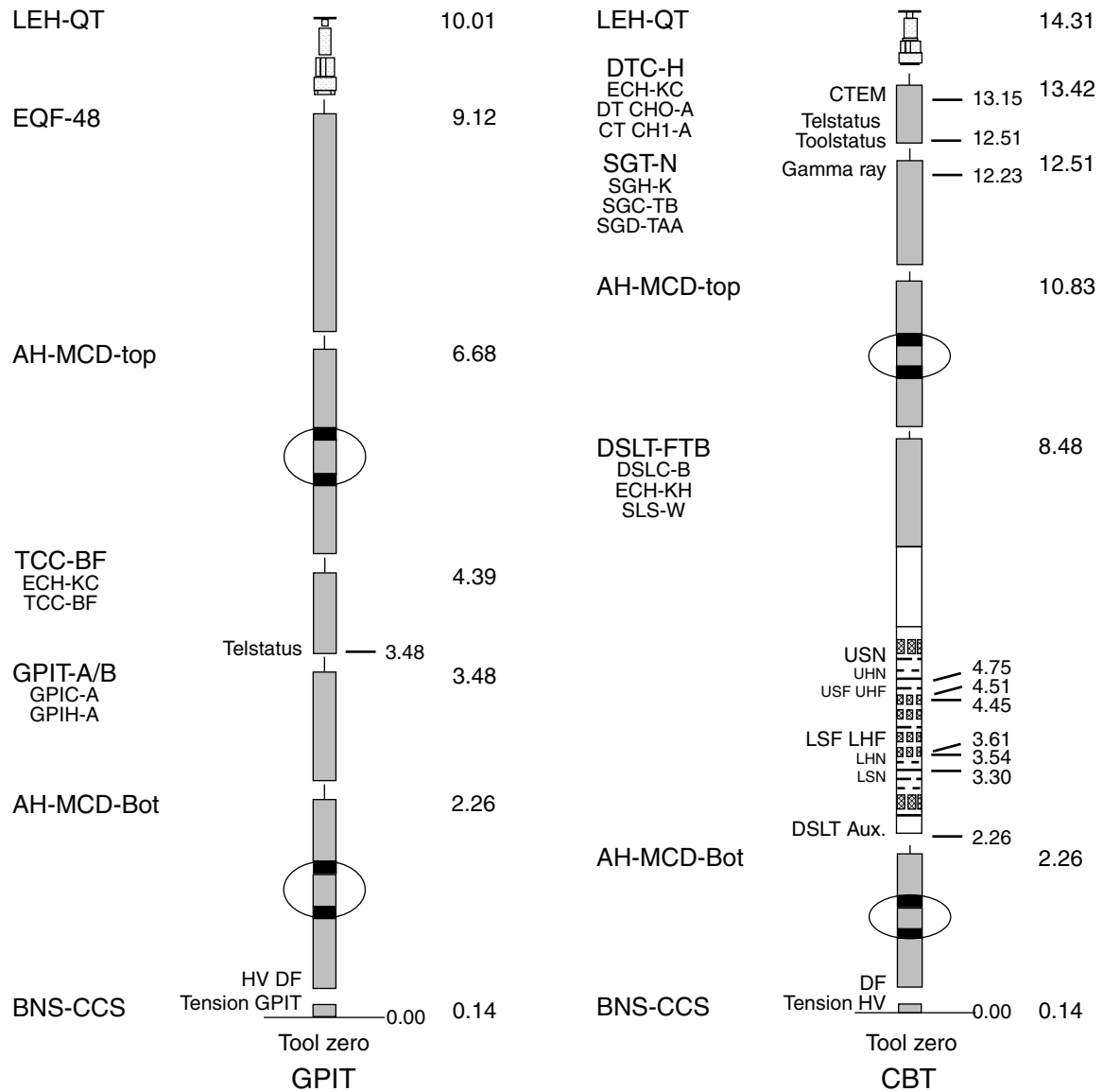


Figure F7. The GPIT and the CBT, which is a DSLT with 3-ft (near) and 5-ft (far) detector spacings.



**Figure F8.** Schematic diagram of a gun configuration as used during Leg 203. The gun used is a Sodera 210-in<sup>3</sup> GI air gun operating in harmonic mode (redrawn from Seismic Systems Manual, 2000). Two hydrophones were suspended together with the gun. One was attached on the gun itself and the other ~2 m below it. When the gun fires, the emitted sound wave is recorded by the hydrophones as a break signal. The signal in the WST sonde geophone is recorded in full wave form. GI = generator-injector gun.

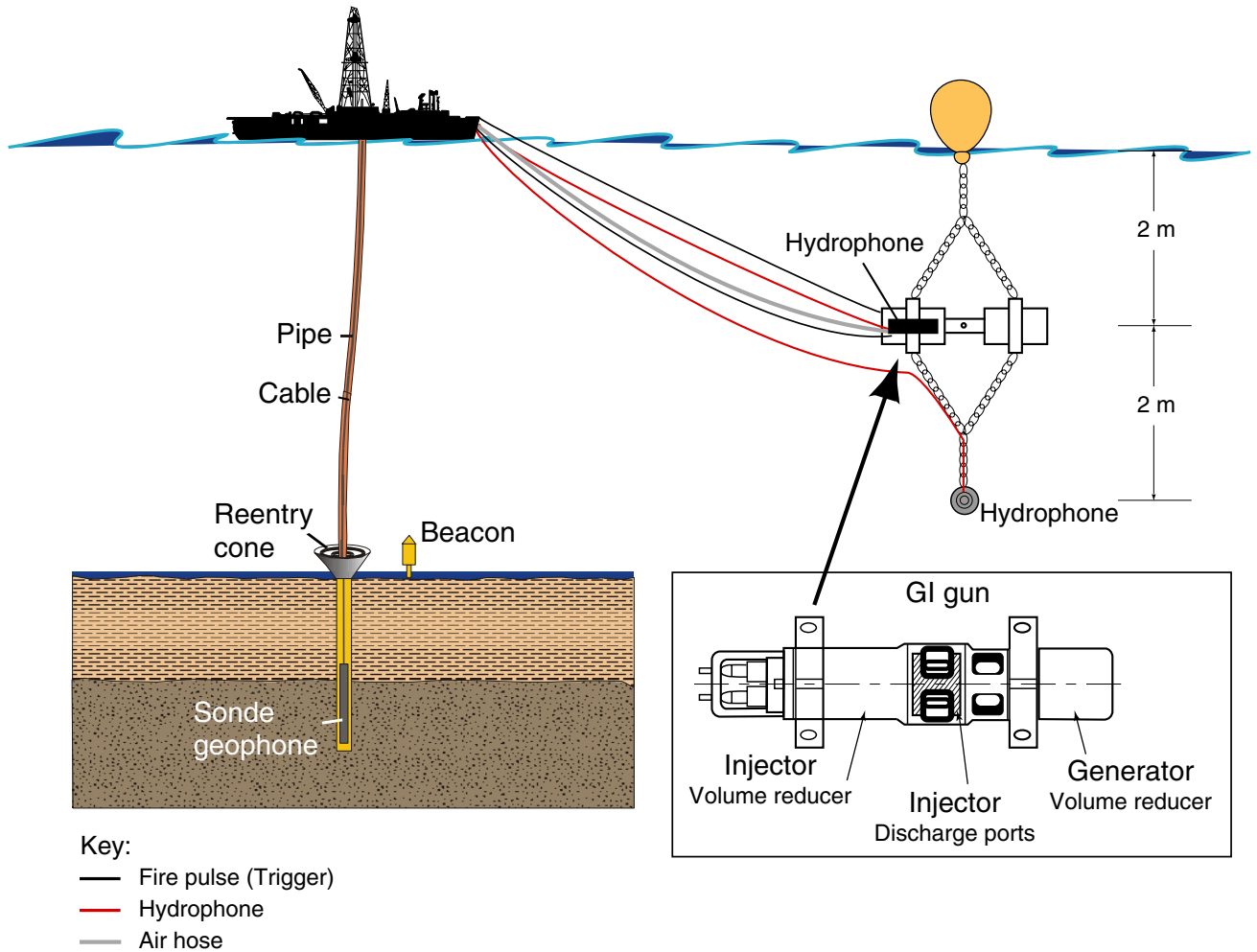
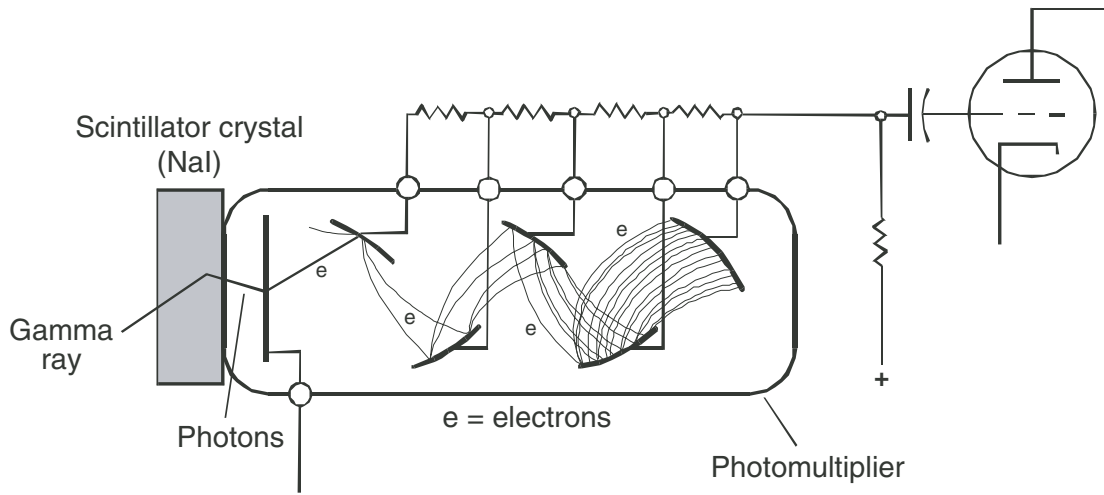


Figure F9. Schematic drawing of a gamma ray tool (redrawn from Serra, 1979).





**Figure F10.** A. Schematic drawing of Compton scattering of gamma rays. The effect is more marked in denser matter (cf. Lavenda, 1985). B. Density and lithodensity (photoelectric) logging in relation gamma ray energy. Density logging uses the high-energy regions where Compton scattering occurs. Photoelectric logging uses the low-energy region where the PEF is dominant. cps = counts per second,  $Z$  = atomic number (modified from Ellis, 1987).

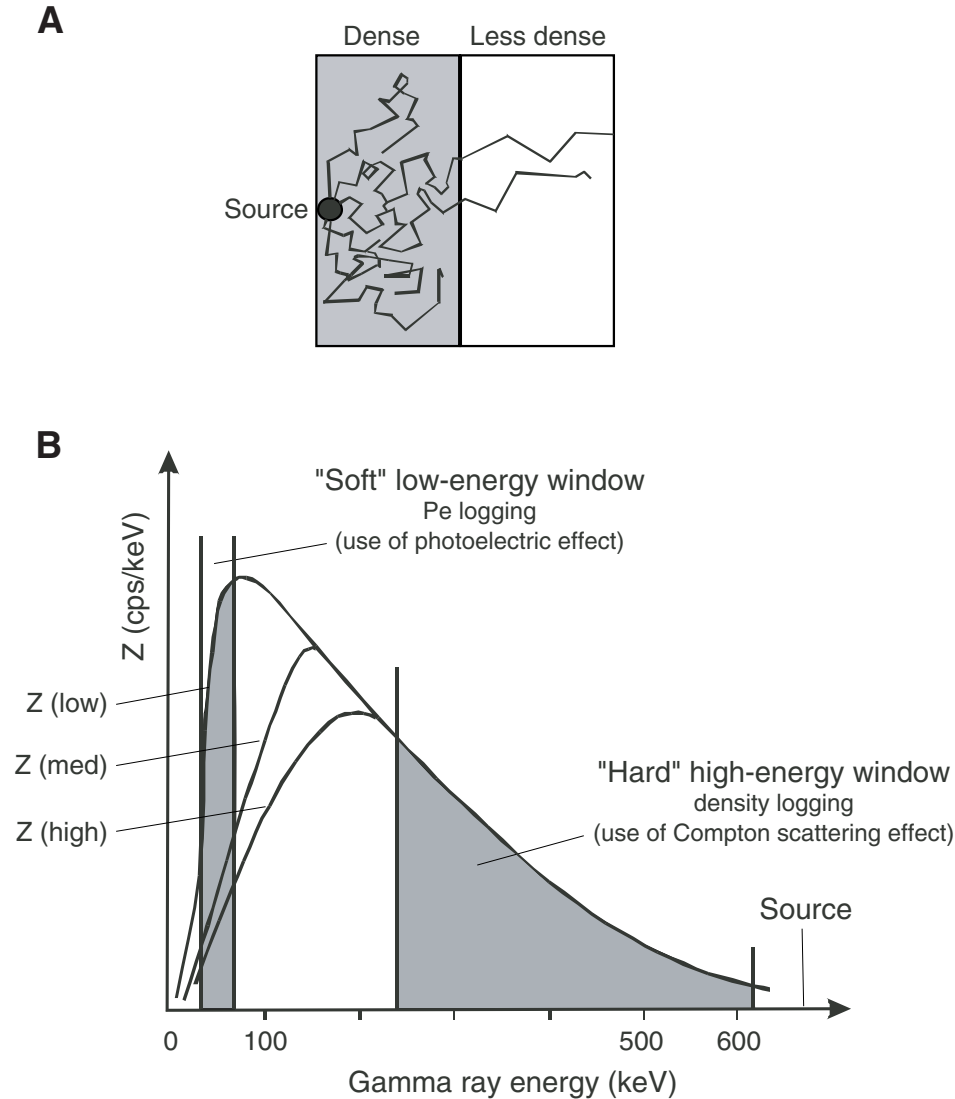
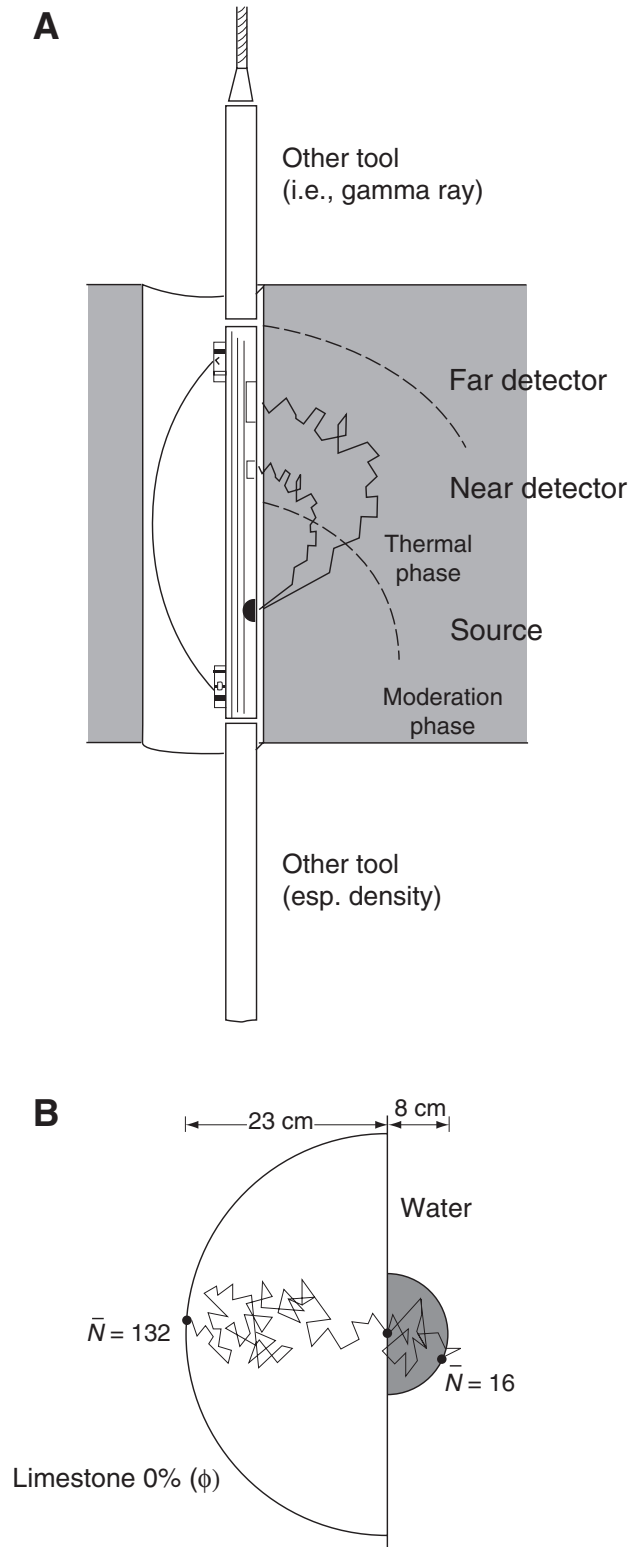
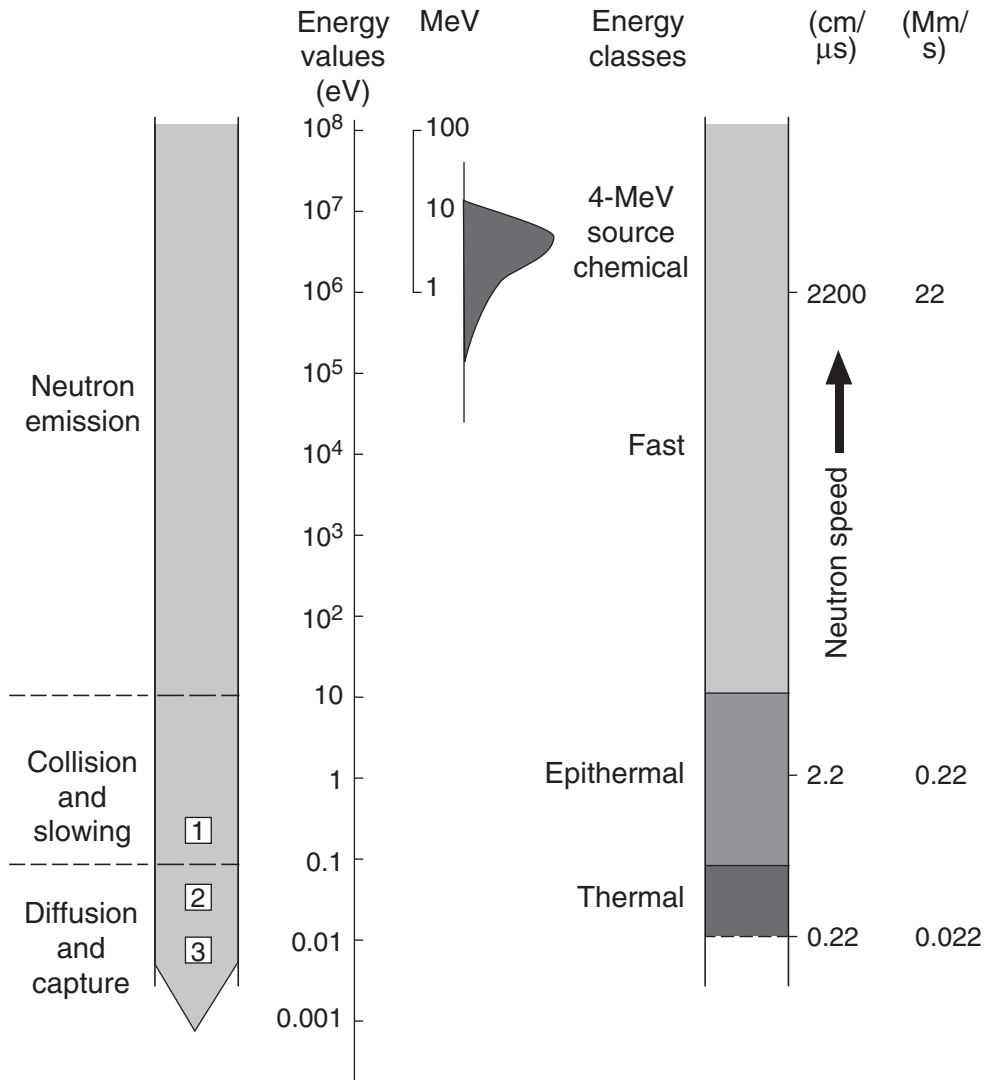


Figure F11. A. Compensated neutron tool schematic drawing. The source and detectors are held pressed against the borehole wall (redrawn from Rider, 1996). B. Schematic trajectories of a neutron in a limestone with no porosity and pure water. The slowing down length in a limestone is far greater than in water (modified from Ellis, 1987).



**Figure F12.** Schematic diagram of a neutron life, showing the energy degradation after emission and the neutron tool detector levels (from Serra, 1979; Tittle, 1961; Owen, 1966).



Detectors for:

- 1 Epithermal neutrons
- 2 Thermal neutrons
- 3 Gamma rays

Figure F13. The principle of the simple induction tool. The vertical component of the magnetic field from the transmitting coil (T) induces a ground loop in the formation, which, in turn, is detected by the receiver coil (R) (redrawn, modified from Ellis, 1987).

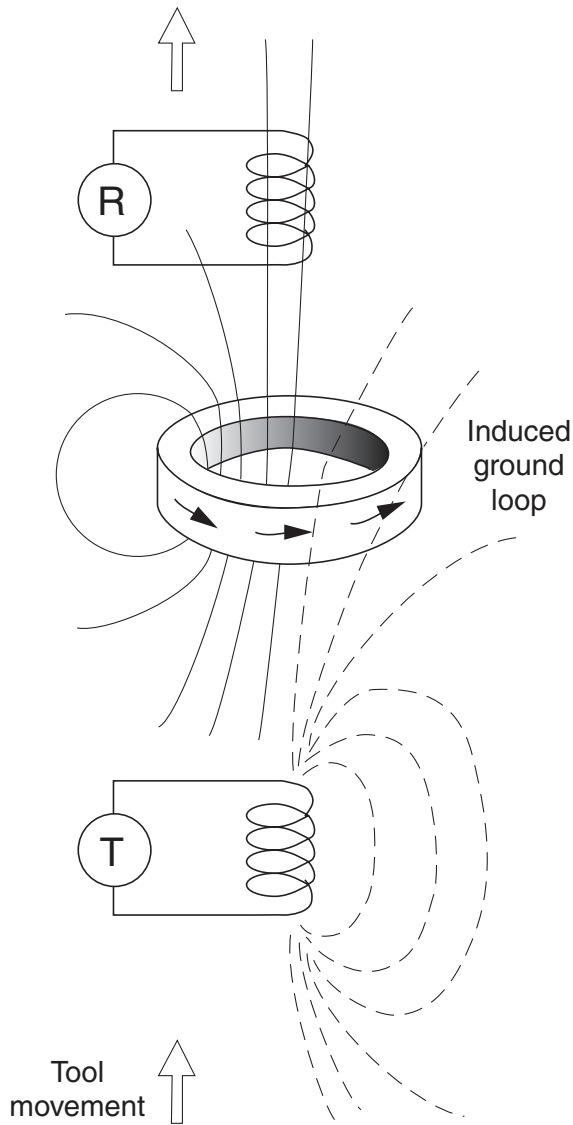


Figure F14. Illustration of the principle of the spontaneous potential (SP) log. A natural potential is measured between an electrode in the well and earth at the surface (redrawn from Rider, 1996).

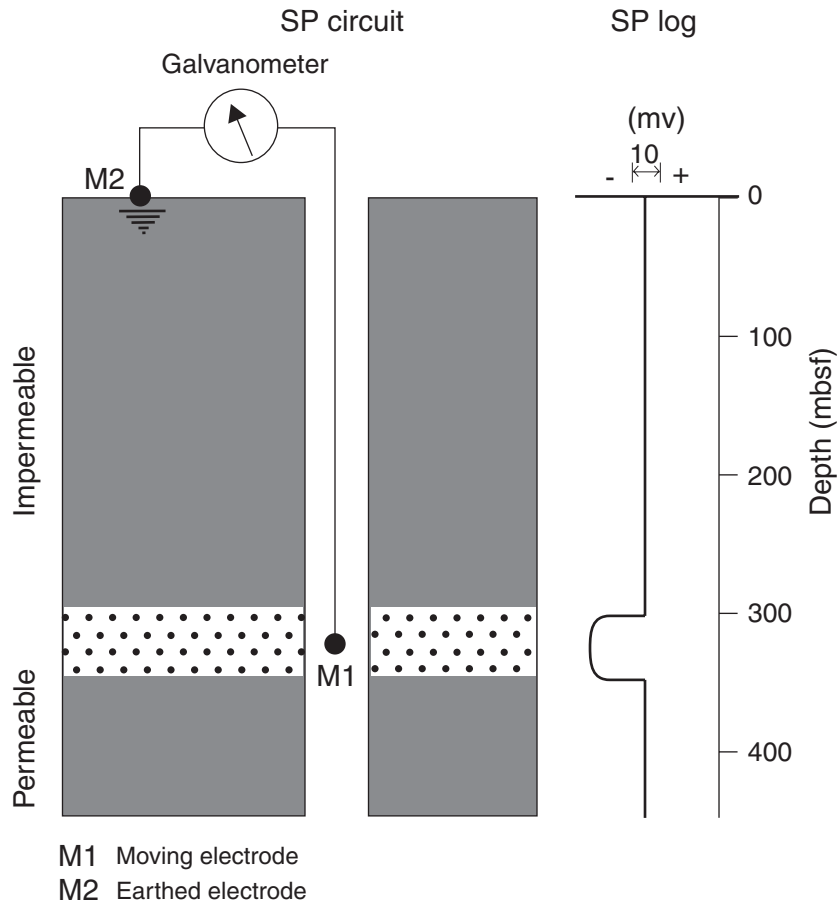
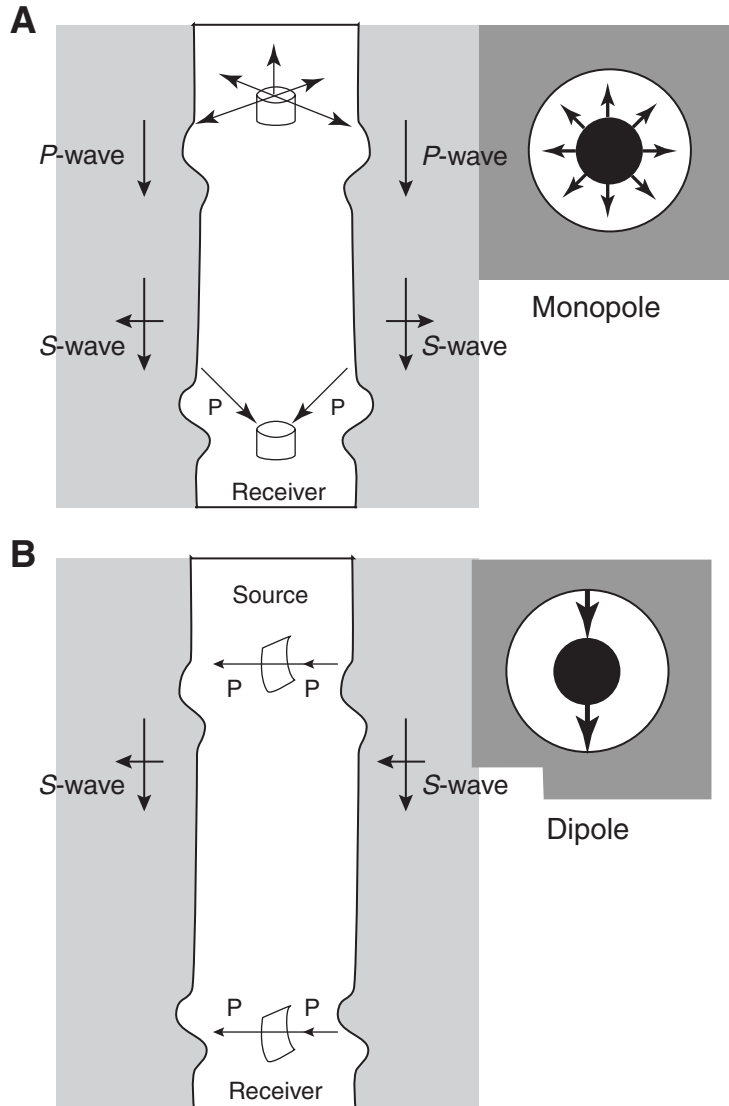


Figure F15. Array sonic transmitter types. A. Monopole transmitter giving a multidirectional pulse. B. Dipole transmitter giving a directed pulse (modified from Zemanek et al., 1991).



**Figure F16.** Schematic diagram of Schlumberger (A) FMS with four pads, 16 buttons each pad, covering 25%–40% of hole diameter (8½ in) and (B) Fullbore Formation MicroImager (FM) with four pads and 24 buttons on each pad. The hinged flap is able to increase coverage of up to 80% (redrawn from Ekstrom et al., 1987; Schlumberger, 1994b). The individual buttons are aligned in two rows; processes for depth corrections shift the recorded resistivity to one row. Each button consists of an electrode surrounded by an insulation.

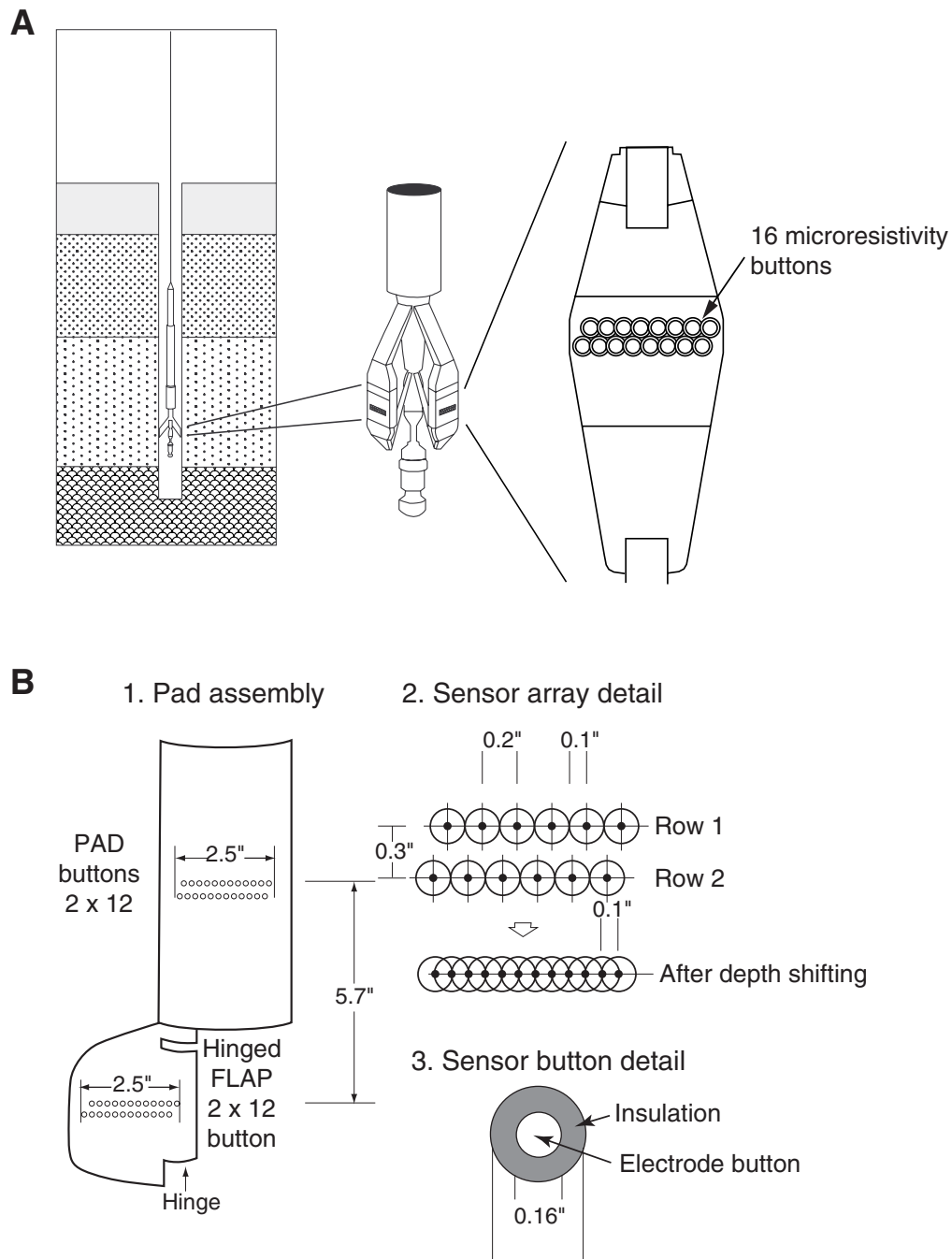
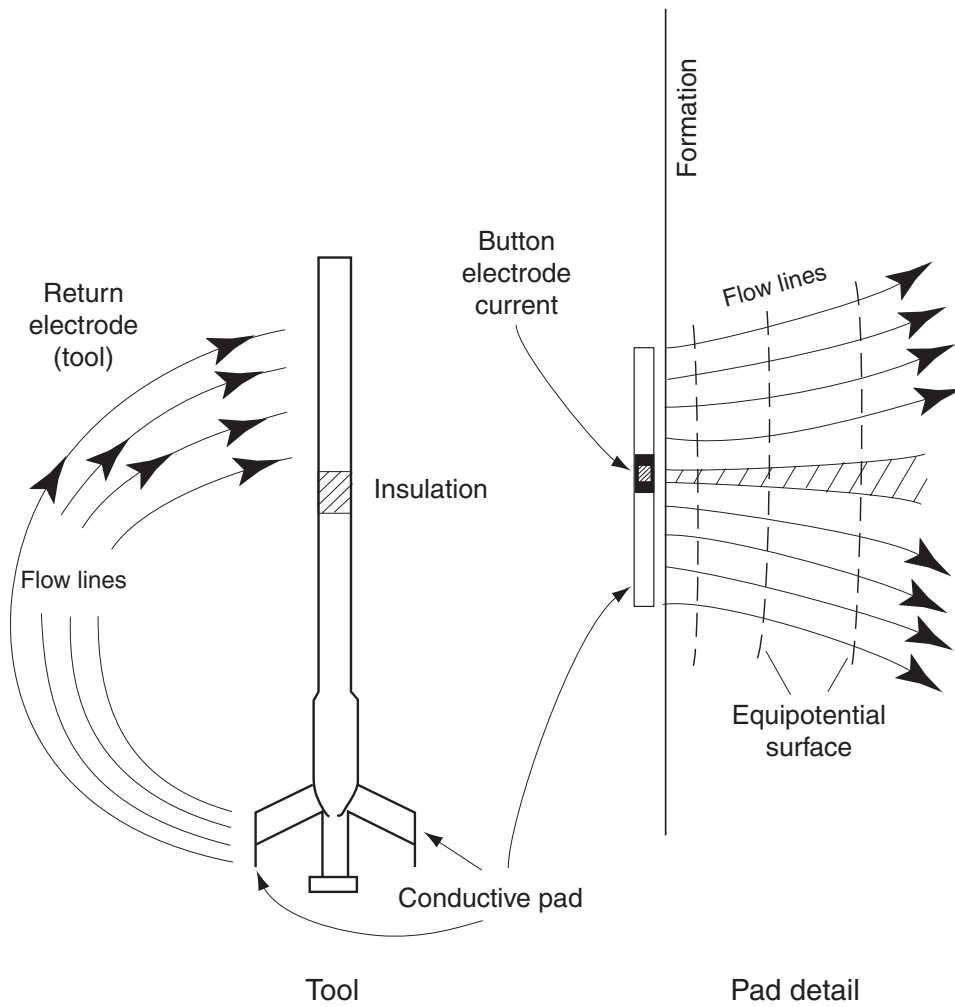
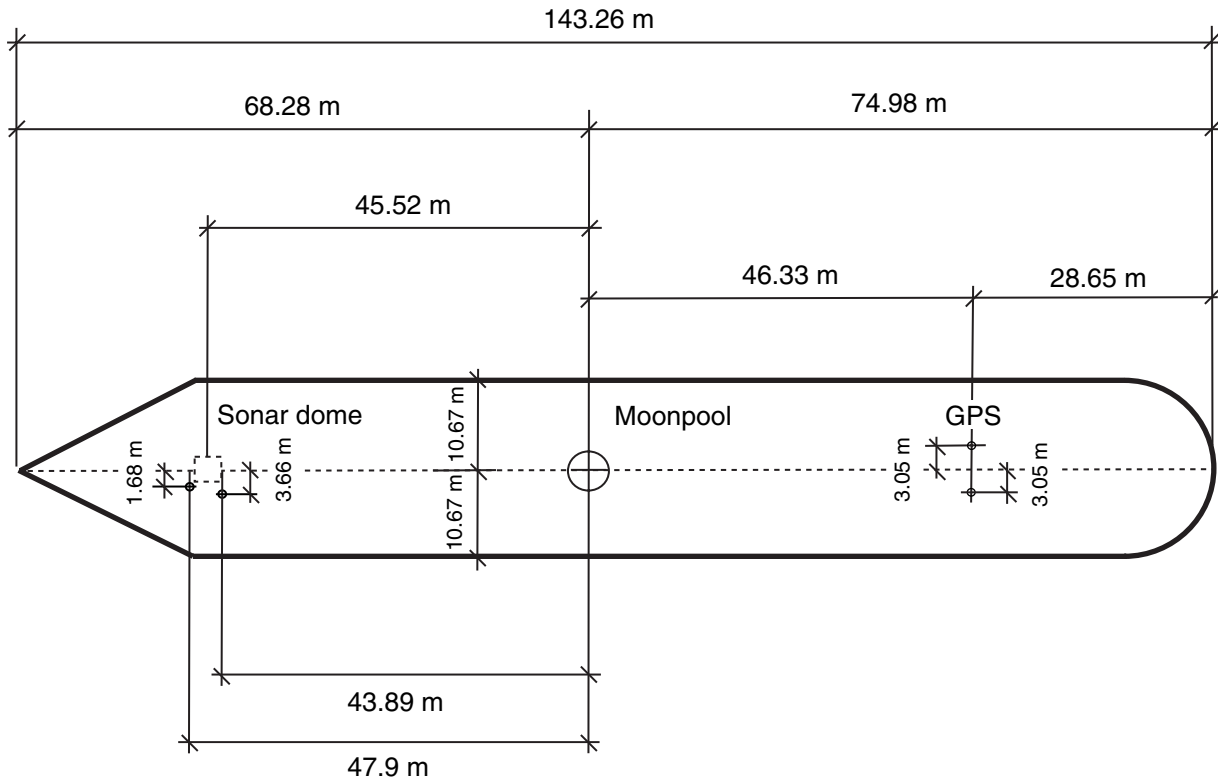


Figure F17. Electrical flow characteristics of an electrical imaging tool (based on the FMI of Schlumberger) (redrawn and modified from Ekstrom et al., 1987, and Schlumberger, 1994b).





**Figure F18.** This figure, which is a modified version of a figure that has been available on the ship for many years, summarizes the significant dimensions necessary to correct the Global Positioning System (GPS) location of various antennas to the moonpool. fwd = forward, stbd = starboard.



**WINFROG ship configuration**

Width of bow = 0.5 m  
 Width of stern = 21.34 m

Origin to bow = 68.28 m  
 Origin to stern = 74.98 m  
 Origin to bow curve = 45.52 m  
 Origin to starboard side = 10.67 m  
 Origin to port side = -10.67 m

Moonpool width = 5.0 m  
 Moonpool fwd/aft = 0.0 m  
 Moonpool port/stbd = 0.0 m

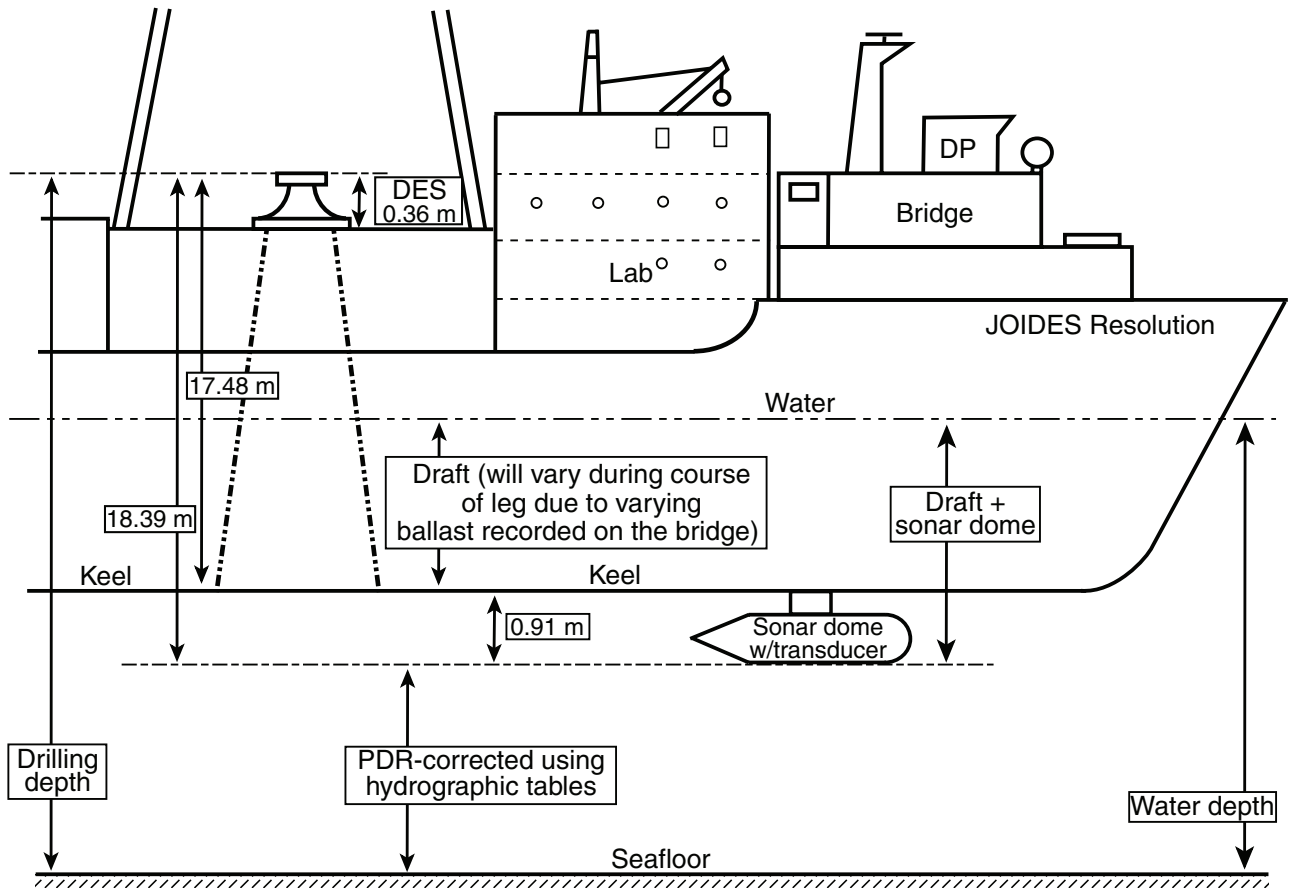
GPS antenna offset from origin  
 Antenna fwd/aft = -46.33 m  
 Antenna (OMNISTAR) port/stbd = 3.05 m  
 Antenna (Ashtech) port/stbd = -3.05 m

**Dynamic Positioning GPS antennas**

Trimble GPS antenna offset from origin  
 Antenna fwd/aft = 47.9 m  
 Antenna port/stbd = -1.68 m

Ashtech GPS antenna offset from origin  
 Antenna fwd/aft = 43.89 m  
 Antenna port/stbd = -3.66 m

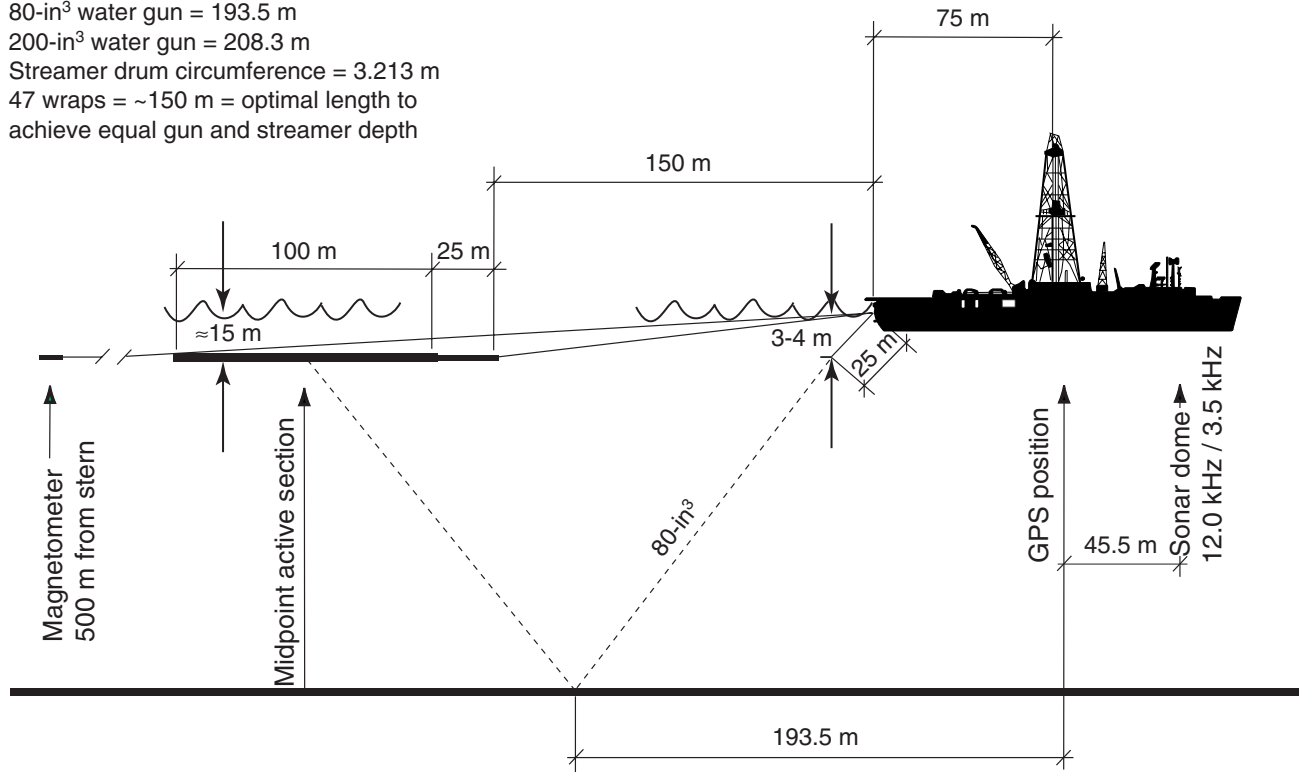
Figure F19. This figure, which has been available on the ship for many years, summarizes some of the significant depth dimensions on the ship. The drillers commonly use the depth below the dual elevator stool (DES). The echo sounder depth corrected by Matthews' tables gives the depth to the sonar dome. DP = dynamic positioning room, PDR = precision depth recorder.



**Figure F20.** This figure, which has been available on the ship for many years, summarizes the significant depths and ranges for the single-channel seismic acquisition system and magnetometer system on board the *JOIDES Resolution*.

**WINFROG streamer vehicle offset**

80-in<sup>3</sup> water gun = 193.5 m  
 200-in<sup>3</sup> water gun = 208.3 m  
 Streamer drum circumference = 3.213 m  
 47 wraps = ~150 m = optimal length to achieve equal gun and streamer depth



**Table T1.** Inductively coupled plasma–atomic emission spectroscopy run parameters.

Element	Instrument detection limit (ppb)	Wavelength (nm)	Slit width (nm)*	Integration time/calculation point (s)	Voltage (V)	Mode	Increment between points (nm) <sup>†</sup>	Calculation (points)
Al	2.8	396.152	20/15	1.0	660	Gauss	0.0030	5
Ca	0.2	393.366	20/15	1.0	320	Gauss	0.0030	5
Fe	6.2	259.940	20/15	4.0	670	Max	0.0030	1
K	60	766.490	20/15	1.0	920	Gauss	0.0030	5
Mg	1.6	285.213	20/15	4.0	710	Max	0.0030	1
Mn	1.4	257.610	20/15	4.0	690	Max	0.0030	1
Na	69	589.592	20/15	1.0	570	Gauss	0.0030	5
P	272	178.229	20/15	1.0	990	Max	0.0030	1
Si	12	251.611	20/15	1.0	680	Gauss	0.0030	5
Ti	3.8	334.941	20/15	1.0	690	Gauss	0.0030	5
Ba	1.3	455.403	20/15	4.0	580	Max	0.0030	1
Co	6	238.892	20/15	1.0	650	Gauss	0.0030	5
Cr	7	267.716	20/15	4.0	740	Max	0.0030	1
Cu	5.4	324.754	20/15	1.0	650	Gauss	0.0030	5
Nb	36	316.340	20/15	1.0	670	Max	0.0030	5
Ni	15	231.604	20/15	1.0	900	Max	0.0020	1
Sc	1.5	361.384	20/15	4.0	590	Max	0.0030	1
Sr	0.4	407.771	20/15	1.0	670	Gauss	0.0030	5
V	7.5	292.402	20/15	4.0	860	Max	0.0030	1
Y	3.5	371.029	20/15	4.0	620	Max	0.0030	1
Zn	1.8	213.856	20/15	1.0	930	Max	0.0030	5
Zr	71	343.823	20/15	1.0	610	Gauss	0.0030	5

Notes: \* = widths of the entrance and exit slits. † = interval between each of the calculation points in Gauss mode or the calculation window that constitutes the single point in Max mode. This table is also available in [ASCII](#).

**Table T2.** Rock standard analyzed.

	BHVO-2	BHVO-2	BHVO-2	Average	Certified value	BIR-1	BIR-1	BIR-1	Average	Certified value	JB-1	JB-1	JB-1	Average	Certified value
Major element oxide (wt%):															
Run #	1	2	3			1	2	3			1	2	3		
SiO <sub>2</sub>	48.63	48.05	48.18	48.29	49.85	46.07	47.40	46.66	46.71	47.95	54.80	54.22	54.72	54.58	52.16
TiO <sub>2</sub>	2.68	2.67	2.70	2.68	2.69	0.92	0.96	0.89	0.93	0.96	1.34	1.33	1.33	1.33	1.3
Al <sub>2</sub> O <sub>3</sub>	13.53	12.92	13.36	13.27	13.85	15.07	15.80	15.49	15.45	15.50	15.18	15.00	14.96	15.05	14.51
Fe <sub>2</sub> O <sub>3t</sub>	11.79	12.28	12.36	12.14	12.23	11.87	11.16	10.75	11.26	11.30	8.79	9.19	9.45	9.14	9.1
MnO	0.16	0.17	0.16	0.17	0.17	0.20	0.18	0.18	0.18	0.18	0.13	0.15	0.16	0.15	0.15
MgO	6.90	6.75	6.64	6.76	7.31	9.80	9.56	9.47	9.61	9.70	7.67	8.12	8.32	8.03	7.75
CaO	11.29	11.24	11.28	11.27	11.33	12.95	12.89	12.85	12.90	13.30	9.67	9.82	9.84	9.77	9.23
Na <sub>2</sub> O	2.17	2.17	2.18	2.17	2.29	1.79	1.83	1.78	1.80	1.82	2.85	2.82	2.85	2.84	2.74
K <sub>2</sub> O	0.51	0.51	0.50	0.51	0.54	0.02	0.02	0.02	0.02	0.03	1.47	1.47	1.47	1.47	1.46
P <sub>2</sub> O <sub>5</sub>	0.23	0.26	0.27	0.25	0.27	0.03	0.00	0.01	0.01	0.02	0.28	0.26	0.26	0.27	0.26
Totals:	97.89	97.02	97.63	97.51	100.53	98.72	99.80	98.10	98.87	100.76	102.18	102.38	103.35	102.64	98.66
Trace element (ppm):															
Ba	127.4	125.8	121.8	125.0	139.00	6.4	6.4	5.9	6.2	7.00	499.2	500.3	500.7	500.0	497
Cr	274.9	284.4	274.6	278.0	289.00	408.4	376.9	368.8	384.7	382.00	393.7	421.8	434.8	416.8	415
Sc	31.1	32.0	31.9	31.7	31.80	45.1	44.1	36.8	42.0	44.00	27.5	28.5	33.4	29.8	29
Sr	385.3	382.8	382.1	383.4	403.00	109.7	104.6	107.7	107.3	108.00	457.1	460.6	460.1	459.3	443
V	335.3	336.1	341.4	337.6	317.00	351.7	349.2	332.7	344.5	313.00	221.0	222.6	237.0	226.9	220
Y	27.4	26.7	26.3	26.8	27.60	17.0	16.9	15.2	16.4	16.00	23.2	24.3	25.6	24.4	24
Zr	177.4	176.7	175.3	176.5	179.00	15.5	15.7	14.1	15.1	15.50	147.4	148.4	149.9	148.6	146
Zn	101.7	74.8	107.0	94.5	105.00	77.7	82.8	68.8	76.5	71.00	75.0	93.5	79.7	82.7	82
Co	50.4	50.1	50.4	50.3	45.00	46.5	46.9	46.4	46.6	52.00	38.9	38.9	39.2	39.0	39.5
Cu	151.5	152.0	152.6	152.0	136.00	53.0	54.6	53.0	53.5	126.00	75.4	74.9	73.6	74.6	55.5
Nb	23.8	23.7	23.8	23.8	19.00	BDL	BDL	BDL		0.60	11.6	11.7	11.8	11.7	27
Ni	112.2	105.8	109.0	109.0	121.00	29.4	34.0	112.0	58.4	166.00	30.6	29.0	137.2	65.6	140

Notes: BDL = below detection limit. This table is also available in [ASCII](#).

**Table T3.** Measurements made by wireline tool strings.

Tool string	Tool	Measurement	Sampling interval (cm)	Approximate vertical resolution (cm)
Triple combination	HNGS*	Spectral gamma ray	15	51
	APS	Porosity	5 and 15	43
	HLDS/HLDT	Bulk density	2.5 and 15	38/46
	DIT/DLL	Resistivity	15	200/150/76, 61(dll)
	TAP	Temperature	1 per s	NA
		Tool acceleration	4 per s	NA
		Pressure	1 per s	NA
		MGT†	Gamma ray	15
Formation MicroScanner	NGT	Spectral gamma ray	15	46
(FMS)-sonic combination	GPIT	Tool orientation	0.25 and 15	NA
	FMS	Microresistivity	0.25	0.5
	DSI/SDT/LSS/BHC	Acoustic velocity	15	107/120/61/61
GHMT	NGT	Spectral gamma ray	15	46
	SUMS	Susceptibility	5 and 15	35
	NMRS	Total field	5 and 15	45
Borehole televiewer	BHTV	Sonic imaging	Variable	1.5–8
WST (stationary measurement)	WST	Sonic traveltime	Variable	NA

Notes: All tool and tool string names (except the TAP and MGT tools) are trademarks of Schlumberger. For additional information about tool physics and use consult ODP Logging Services at [www.ideo.columbia.edu/BRG/ODP](http://www.ideo.columbia.edu/BRG/ODP). \* = see Table T4, p. 55, for explanations of acronyms used to describe tool strings and tools. † = not included in each logging run. NA = not applicable.

**Table T4.** Acronyms and units used for wireline logging tools.

Tool	Output	Explanation	Units
APS		Accelerator Porosity Sonde	
	APLC	Near array porosity (limestone calibrated)	%
	SIGF	Formation capture cross section ( $\Sigma_p$ )	Capture units
	STOF	Tool standoff (computed distance from borehole wall)	in
BHC		Borehole Compensated Sonic tool	
	DT	Compressional wave delay time ( $\Delta t$ )	ms/ft
DIT		Dual Induction Tool	
	IDPH	Deep induction resistivity	$\Omega m$
	IMPH	Medium induction resistivity	$\Omega m$
	SFLU	Spherically focused resistivity	$\Omega m$
DLL		Dual Laterolog	
	LLD	Deep resistivity	$\Omega m$
	LLS	Shallow resistivity	$\Omega m$
DSI		Dipole Sonic Imager	
	DTCO	Compressional wave delay time ( $\Delta t$ )	ms/ft
	DTSM	Shear wave delay time ( $\Delta t$ )	ms/ft
	DTST	Stoneley wave delay time ( $\Delta t$ )	ms/ft
FMS		Formation MicroScanner	
	C1, C2	Orthogonal hole diameters	in
	P1AZ	Pad 1 azimuth	Degrees
		Spatially oriented resistivity images of borehole wall	
GHMT		Geologic High-Resolution Magnetic tool	
	MAGS	Magnetic susceptibility (limited range)	ppm
	RMGS	Low-resolution magnetic susceptibility (wider range)	ppm
	MAGC	Earth's conductivity	ppm
GPIT		General Purpose Inclinometer Tool	
	DEVI	Hole deviation	Degrees
	HAZI	Hole azimuth	Degrees
	$F_x, F_y, F_z$	Earth's magnetic field (three orthogonal components)	Degrees
	$A_x, A_y, A_z$	Acceleration (three orthogonal components)	$m/s^2$
HLDS		Hostile Environment Litho-Density Sonde	
	RHOM	Bulk density	$g/cm^3$
	PEFL	Photoelectric effect	$b/e^-$
	LCAL	Caliper (measure of borehole diameter)	in
HLDT		Hostile Environment Litho-Density Tool	
	RHOB	Bulk density (corrected)	$g/cm^3$
	PEF	Photoelectric effect	$b/e^-$
	CALI	Caliper (measure of borehole diameter)	in
	DRHO	Bulk density correction	$g/cm^3$
HNGS		Hostile Environment Gamma Ray Sonde	
	HSGR	Standard (total) gamma ray	gAPI
	HCGR	Computed gamma ray (HSGR minus uranium contribution)	gAPI
	HFK	Potassium	wt%
	HTHO	Thorium	ppm
LSS		Long Spacing Sonic tool	
	DT	Short-spacing delay time ( $\Delta t$ )	$\mu s/ft$
MGT		Multi-sensor Spectral Gamma Ray tool	
	GR	Gamma ray	gAPI
NGT		Natural Gamma Ray Spectrometry Tool	
	SGR	Standard total gamma ray	gAPI
	CGR	Computed gamma ray (SGR minus uranium contribution)	gAPI
	POTA	Potassium	wt%
	THOR	Thorium	ppm
	URAN	Uranium	ppm
SDT		Digital Sonic Tool	
	DTCO	Compressional wave delay time ( $\Delta t$ )	$\mu s/ft$
TAP		Temperature/acceleration/pressure tool	$^{\circ}C, m/s^2, psi$
WST		Well Seismic Tool	
		Acoustic arrival times	ms